nature medicine

LETTERS

https://doi.org/10.1038/s41591-020-1008-z

Check for updates

Implications of *TP53* allelic state for genome stability, clinical presentation and outcomes in myelodysplastic syndromes

Elsa Bernard[1,2], Yasuhito Nannya[3], Robert P. Hasserjian[4], Sean M. Devlin[5], Heinz Tuechler[6], Juan S. Medina-Martinez[1,2], Tetsuichi Yoshizato[3], Yusuke Shiozawa[3], Ryunosuke Saiki[3], Luca Malcovati[7,8], Max F. Levine[1,2], Juan E. Arango[1,2], Yangyu Zhou[1,2], Francesc Solé[9], Catherine A. Cargo[10], Detlef Haase[11], Maria Creignou[12], Ulrich Germing[13], Yanming Zhang[14], Gunes Gundem[1], Araxe Sarian[2], Arjan A. van de Loosdrecht[15], Martin Jädersten[12], Magnus Tobiasson[12], Olivier Kosmider[16], Matilde Y. Follo[17], Felicitas Thol[18], Ronald F. Pinheiro[19], Valeria Santini[20], Ioannis Kotsianidis[21], Jacqueline Boultwood[22], Fabio P. S. Santos[23], Julie Schanz[11], Senji Kasahara[24], Takayuki Ishikawa[25], Hisashi Tsurumi[26], Akifumi Takaori-Kondo[27], Toru Kiguchi[28], Chantana Polprasert[29], John M. Bennett[30], Virginia M. Klimek[31], Michael R. Savona[32], Monika Belickova[33], Christina Ganster[11], Laura Palomo[9], Guillermo Sanz[34,35], Lionel Ades[36], Matteo Giovanni Della Porta[37], Alexandra G. Smith[38], Yesenia Werner[1], Minal Patel[2], Agnès Viale[39], Katelynd Vanness[39], Donna S. Neuberg[40], Kristen E. Stevenson[40], Kamal Menghrajani[31], Kelly L. Bolton[31], Pierre Fenaux[36], Andrea Pellagatti[22], Uwe Platzbecker[41], Michael Heuser[18], Peter Valent[42], Shigeru Chiba[43], Yasushi Miyazaki[44], Carlo Finelli[45], Maria Teresa Voso[46], Lee-Yung Shih[47], Michaela Fontenay[16], Joop H. Jansen[48], José Cervera[49], Yoshiko Atsuta[50], Norbert Gattermann[13], Benjamin L. Ebert[51], Rafael Bejar[52], Peter L. Greenberg[53], Mario Cazzola[7,8], Eva Hellström-Lindberg[12], Seishi Ogawa[3,54] and Elli Papaemmanuil[1,2,54] ✉

Tumor protein p53 (*TP53*) is the most frequently mutated gene in cancer[1,2]. In patients with myelodysplastic syndromes (MDS), *TP53* mutations are associated with high-risk disease[3,4], rapid transformation to acute myeloid leukemia (AML)[5], resistance to conventional therapies[6–8] and dismal outcomes[9]. Consistent with the tumor-suppressive role of *TP53*, patients harbor both mono- and biallelic mutations[10]. However, the biological and clinical implications of *TP53* allelic state have not been fully investigated in MDS or any other cancer type. We analyzed 3,324 patients with MDS for *TP53* mutations and allelic imbalances and delineated two subsets of patients with distinct phenotypes and outcomes. One-third of *TP53*-mutated patients had monoallelic mutations whereas two-thirds had multiple hits (multi-hit) consistent with biallelic targeting. Established associations with complex karyotype, few co-occurring mutations, high-risk presentation and poor outcomes were specific to multi-hit patients only. *TP53* multi-hit state predicted risk of death and leukemic transformation independently of the Revised International Prognostic Scoring System (IPSS-R)[11]. Surprisingly, monoallelic patients did not differ from *TP53* wild-type patients in outcomes and response to therapy. This study shows that consideration of *TP53* allelic state is critical for diagnostic and prognostic precision in MDS as well as in future correlative studies of treatment response.

In collaboration with the International Working Group for Prognosis in MDS (Supplementary Table 1), we assembled a cohort of 3,324 peridiagnostic and treatment-naive patients with MDS or closely related myeloid neoplasms (Extended Data Fig. 1 and Supplementary Fig. 1). Genetic profiling included conventional G-banding analyses (CBA) and tumor-only, capture-based, next-generation sequencing (NGS) of a panel of genes recurrently mutated in MDS, as well as genome-wide copy number probes. Allele-specific copy number profiles were generated from NGS data using the CNACS algorithm[7] (see Methods and Code availability). An additional 1,120 samples derived from the Japanese MDS consortium (Extended Data Fig. 2) were used as a validation cohort.

To study the effect of *TP53* allelic state on genome stability, clinical presentation, outcome and response to therapy, we performed a detailed characterization of alterations at the *TP53* locus. First, we assessed genome-wide allelic imbalances in the cohort of 3,324 patients, to include arm-level or focal (~3 Mb) ploidy alterations and regions of copy-neutral loss of heterozygosity (cnLOH) (Extended Data Fig. 3, Supplementary Figs. 2–4 and Methods).

A full list of affiliations appears at the end of the paper.

Collectively, 360 (11%) patients had at least one cnLOH region and 1,571 (47%) had at least one chromosomal aberration. Among these, 329 karyotypes were complex[12] and 177 were monosomal[13] (Supplementary Table 2).

Mutation analysis identified 486 putative oncogenic mutations in *TP53* at variant allele frequency (VAF) ≥ 2% across 378 individuals (Supplementary Figs. 5–7 and Methods). Among *TP53*-mutated patients, 274 (72.5%) had a single *TP53* mutation, 100 had two (26.5%) and four (1%) had three. Allelic imbalances overlapping the *TP53* locus were found in 177 cases. Of these, 98 were focal deletions or regions of cnLOH detected by NGS only (Supplementary Table 3). Approximately half (54%, $n = 149$) of patients with one *TP53* mutation had loss of the wild-type allele by deletion or cnLOH. In contrast, only 13% ($n = 14$) of patients with more than one *TP53* mutation had a concomitant allelic imbalance at the *TP53* locus (odds ratio (OR) = 7.6, 95% confidence interval (CI): 4.1–15.2) (Fig. 1a). By consideration of mutations and allelic imbalances, we defined four *TP53*-mutant subgroups (Fig. 1b): (1) monoallelic mutation ($n = 125$, 33% of *TP53*-mutated patients); (2) multiple mutations without deletion or cnLOH affecting the *TP53* locus ($n = 90$, 24%); (3) mutation(s) and concomitant deletion ($n = 85$, 22%); and (4) mutation(s) and concomitant cnLOH ($n = 78$, 21%). Additionally, in 24 patients the *TP53* locus was affected by deletion ($n = 12$), cnLOH ($n = 2$) or isochromosome 17q rearrangement ($n = 10$) without evidence of *TP53* mutations (Fig. 1a).

In subgroups 2–4, clonality estimates of co-occurring mutations or allelic imbalances supported biallelic targeting of *TP53* (Extended Data Fig. 4). In a subset of cases, biallelic targeting was validated by phasing analysis or sequential sampling (Supplementary Fig. 8). Thus, the *TP53* mutant subgroups were organized into two states: (1) monoallelic *TP53* state representing subgroup 1, with one residual wild-type copy of *TP53*, and (2) multi-hit *TP53* state encompassing subgroups 2–4, with at least two *TP53* hits in each patient and probably no residual *TP53*. While most multi-hit samples were confidently assigned as biallelic, we maintained a conservative 'multi-hit' notation.

Accurate determination of allelic state requires LOH mapping, as can be achieved by NGS-based analysis of sequencing panels[7] or more comprehensive sequencing methods (Supplementary Fig. 4). VAF estimates were not sufficient for precise assessment of *TP53* allelic state (Fig. 1c). For example, 19 cnLOH-positive patients had *TP53* VAF ≤ 50% (median 29%, range 3–49%), showing that one-quarter of cnLOH patients would be misassigned as monoallelic on the basis of VAF.

In monoallelic cases, *TP53* mutations were enriched for subclonal presentation (median VAF = 13%, median sample purity = 86%) as compared to *TP53* mutations from patients with multiple mutations, which were predominantly clonal (median VAF = 32%, median sample purity = 85%) (Fig. 1c). Thus *TP53* allelic state—and, by extension, whether a wild-type *TP53* allele is retained—points toward different evolutionary trajectories or potential for clonal dominance. Overall, the spectrum of *TP53* mutations was shared among the two allelic states (Fig. 1d and Supplementary Fig. 9). Of note, truncating mutations were enriched in the multi-hit state (28 versus 14%, OR = 2.3, 95% CI: 1.3–4.2) while hotspot mutations accounted for 25% of mutations in the monoallelic state and 20% in the multi-hit state.

We next assessed profiles of genome stability and patterns of co-mutations for each *TP53* state. The correlation between *TP53* mutations and chromosomal aneuploidies is well established[3,7,14–16]. Overall, 67% ($n = 252$) of *TP53*-mutated cases had at least two chromosomal deletions as compared to 5% ($n = 158$) of wild-type cases (OR = 35, 95% CI: 27–46). Excluding chr17 (which is linked to state definition), there was a significantly higher number of chromosomal aberrations per patient in all multi-hit *TP53* subgroups compared to the monoallelic group (Fig. 2a and Extended Data Fig. 5), and this enrichment was most pronounced for deletions (median four in multi-hit versus one in monoallelic state). In particular, deletion of 5q was observed in 85% of multi-hit patients as opposed to 34% of monoallelic patients (OR = 10, 95% CI: 6.1–18; Supplementary Fig. 10). Taken together, we found a median of six unique chromosomes with aberrations in the multi-hit state and one in the monoallelic state (two-sided Wilcoxon rank-sum test W statistic = 2,395, $P = 1.2 \times 10^{-41}$; Fig. 2b). Our data suggest that residual wild-type *TP53* is critical to the maintenance of genome stability, and that the association between *TP53* and complex karyotype is specific to the multi-hit state (91 versus 13% complex karyotype patients within multi-hit or monoallelic states, OR = 70, 95% CI: 34–150; Fig. 2c).

The total number of oncogenic gene mutations and the pattern of co-mutations were also different among the allelic states. Excluding *TP53*, the number of driver mutations was higher in the monoallelic state compared to the multi-hit *TP53* subgroups (Fig. 2d). Overall, 40% ($n = 102$) of multi-hit patients did not have any identifiable driver mutations other than *TP53*, while 90% ($n = 112$) of monoallelic patients had at least one other driver mutation and 50% ($n = 62$) had at least three. Differences in the pattern of co-mutations were also identified, whereby monoallelic patients were significantly enriched for mutations in *TET2*, *SF3B1*, *ASXL1*, *RUNX1*, *SRSF2*, *JAK2*, *BCOR* and *CBL* (Fig. 2e).

Previous studies have recurrently linked *TP53* mutations to high-risk presentation (complex karyotype, elevated blasts, severe thrombocytopenia) and adverse outcomes[3,4]. These correlations were recapitulated in our study (Supplementary Fig. 11). However, the clinical implications of the allelic state have not been investigated. In our cohort, monoallelic *TP53* patients were less cytopenic (Fig. 3a–c) and had lower percentages of bone marrow blasts compared to multi-hit patients (median 4 versus 9%; Fig. 3d). There was a higher prevalence of lower-risk MDS in monoallelic patients, while the multi-hit state was enriched for higher-risk WHO (World Health Organization) subtypes and poor/very poor IPSS-R categories (Extended Data Fig. 6a,b). Overall survival (OS) and AML transformation were significantly different between the *TP53* allelic states. In multi-hit state, the median OS was 8.7 months (95% CI: 7.7–10.3) whereas it was 2.5 years (95% CI: 2.2–4.9) for monoallelic patients (hazard ratio (HR) = 3.7, 95% CI: 2.7–5.0, $P = 2 \times 10^{-16}$, Wald test). In comparison, wild-type patients had a median OS of 3.5 years (95% CI: 3.4–3.9) (Fig. 3e). The effect of monoallelic *TP53* on OS was not confounded by del(5q) (Supplementary Fig. 12). The 5-year cumulative incidence of AML transformation in the multi-hit and monoallelic states was, respectively, 44 and 21% (HR = 5.5, 95% CI: 3.1–9.6, $P = 5 \times 10^{-9}$, Wald test) (Fig. 3f). Of note, all subgroups (more than one gene mutation, mutation and deletion, mutation and cnLOH) in multi-hit state had equally dismal outcomes (Extended Data Fig. 7a,b). The OS distinction of the two states was significant across WHO classes and IPSS-R risk groups (Extended Data Fig. 6c,d and Supplementary Fig. 13), and multi-hit *TP53* identified patients with poor survival across IPSS-R strata. Because 10% of multi-hit patients were classified as IPSS-R risk very good to intermediate, this shows that assessment of *TP53* allelic state is critical to identification of patients with high-risk disease. In fact, multivariable Cox proportional hazards models that included *TP53* state alongside age of diagnosis, cytogenetic risk score[12] and established predictive features identified multi-hit *TP53* as an independent predictor for the risk of death and AML transformation ($HR_{OS} = 2.04$, 95% CI: 1.6–2.6, $P = 5 \times 10^{-8}$; $HR_{AML} = 2.9$, 95% CI: 1.8–4.7, $P = 7 \times 10^{-6}$, Wald test), whereas monoallelic *TP53* state was not different compared to wild-type *TP53* (Fig. 3g,h). We also evaluated that multi-hit *TP53* and complex karyotype, but not monoallelic *TP53*, are independent predictors of adverse outcome (Supplementary Fig. 14), emphasizing the importance of mapping *TP53* state alongside complex karyotype for accurate risk estimation.

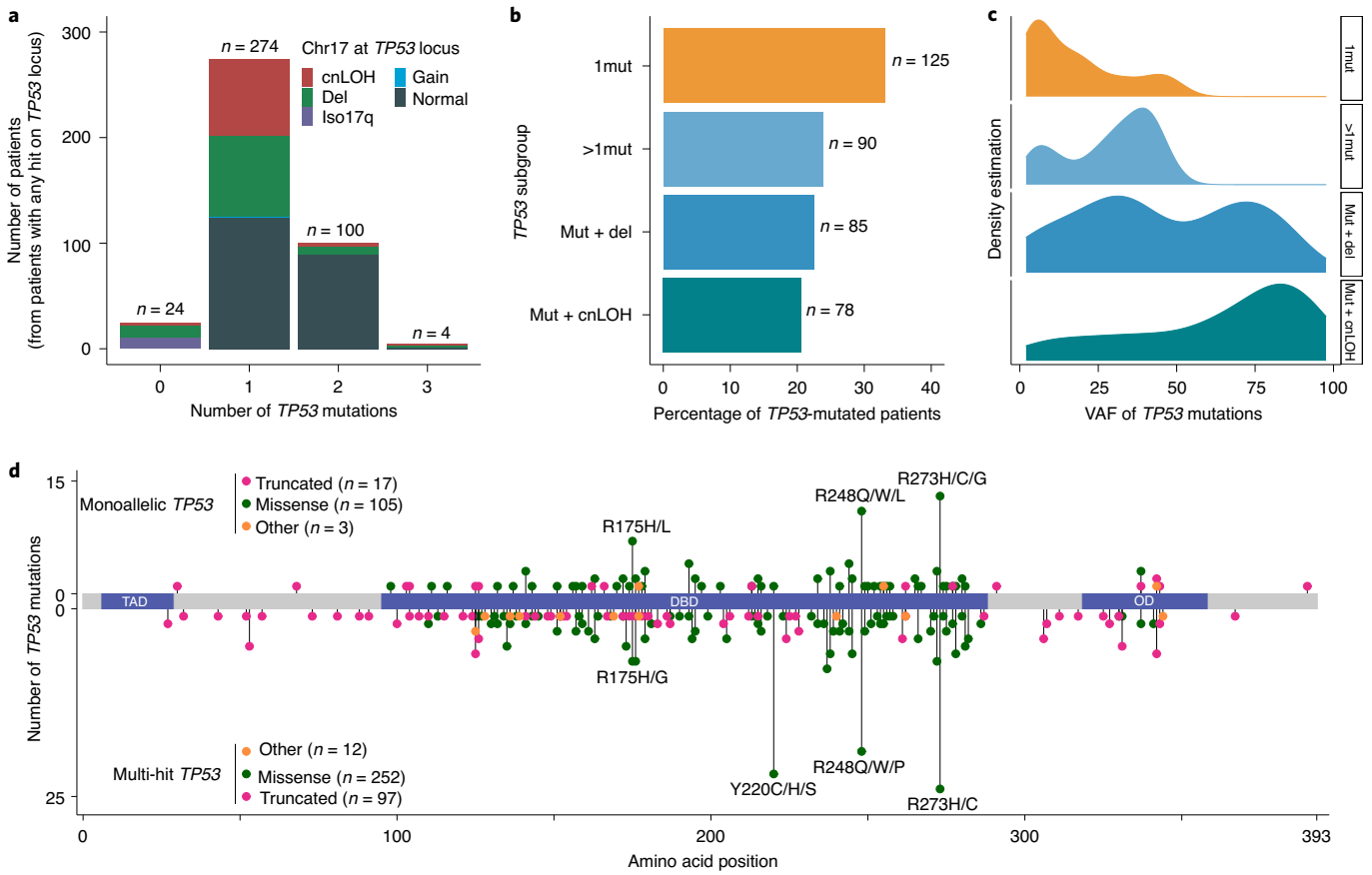

Fig. 1 | Integration of *TP53* mutations and allelic imbalances at the *TP53* locus identifies *TP53* states with evidence of mono- or biallelic targeting. **a**, Number of patients (from patients with any hit at the *TP53* locus) with 0, 1, 2 or 3 *TP53* mutations. Colors represent the status of chromosome 17 at the *TP53* locus, to include cnLOH, deletion (del), isochromosome 17q rearrangement (iso17q), gain or no detected aberration (normal). Unbalanced translocations leading to 17p deletion are encoded as 'del'. **b**, Frequency of *TP53* subgroups within *TP53*-mutated patients. *TP53* subgroups are defined as cases with (1) single gene mutation (1mut); (2) several mutations with normal status of chromosome 17 at the *TP53* locus (>1mut); (3) mutation(s) and chromosomal deletion at the *TP53* locus (mut + del); and (4) mutation(s) and cnLOH at the *TP53* locus (mut + cnLOH). **c**, Density estimation of VAF of *TP53* mutations across *TP53* subgroups (from top to bottom, 1mut, >1mut, mut + del, mut + cnLOH). **d**, Distribution of *TP53* mutations along the gene body. Mutations from patients with monoallelic *TP53* are depicted at the top and those from patients with multiple *TP53* hits at the bottom. Missense mutations are shown as green circles. Truncated mutations corresponding to nonsense or nonstop mutations, frameshift deletions or insertions and splice site variants are shown as pink circles. Other types of mutations to include in-frame deletions or insertions are shown as orange circles. TAD, transactivation domain; OD, oligomerization domain.

Outcomes of monoallelic patients significantly differed with the number of co-occurring driver mutations (Fig. 2d,e and Supplementary Fig. 15). For example, the 5-year survival rate of monoallelic patients with no other identifiable mutations was 81% while it was 36% for patients with one or two other mutations, 26% for patients with three or four other mutations and 8% for patients with more than five other mutations. Contrastingly, the outcome of multi-hit patients was not dependent on the number of additional mutations, and the 5-year survival rate was uniformly <6%. Taken together, multi-hit *TP53* patients had few co-mutations and very poor survival irrespective of genetic context. Patients with monoallelic *TP53* mutations frequently had several co-occurring mutations that shaped disease pathogenesis and outcomes. These data further showcase that monoallelic *TP53* mutations are not independently predictive of adverse risk.

In addition to *TP53* mutations, *TP53* VAF has also been reported to be of prognostic significance in MDS[17–19]. This is probably explained by the strong correlation between high VAF and biallelic targeting. Optimal cut-point analysis[20] identified that patients with monoallelic *TP53* mutations and VAF > 22% ($n = 38$) had increased risk of death compared to wild-type patients (HR = 2.2, 95% CI: 1.5–3.2, $P = 0.0001$, Wald test), whereas patients with monoallelic *TP53* mutations and VAF ≤ 22% ($n = 87$) had OS similar to wild-type patients (Extended Data Fig. 7c). This highlights that patients with monoallelic mutations and high VAF should be closely monitored. It is possible that we missed a second *TP53* hit in the small subset of monoallelic cases with VAF > 22%. Conversely, multi-hit patients had poor outcomes across ranges of VAF. Multi-hit patients with VAF ≤ 11% ($n = 20$) had very dismal outcomes, for both OS and AML transformation (Extended Data Fig. 7c,d). Importantly, the genomic and clinical associations established for multi-hit cases held true irrespective of VAF. Patients with multi-hit *TP53* had higher genome instability, fewer cooperating mutations and more pronounced thrombocytopenia and elevated blast counts compared to monoallelic patients in both clonal and subclonal ranges (Supplementary Fig. 16). This indicates that, once established, a clone with biallelic *TP53* targeting exerts its pervasive effects on clinical phenotypes and outcomes regardless of its size. The determination of *TP53* allelic state requires assessment of both multiple mutations and subclonal allelic imbalances, and multi-hit *TP53* state identified very-high-risk patients independently of the VAF of *TP53* mutations.

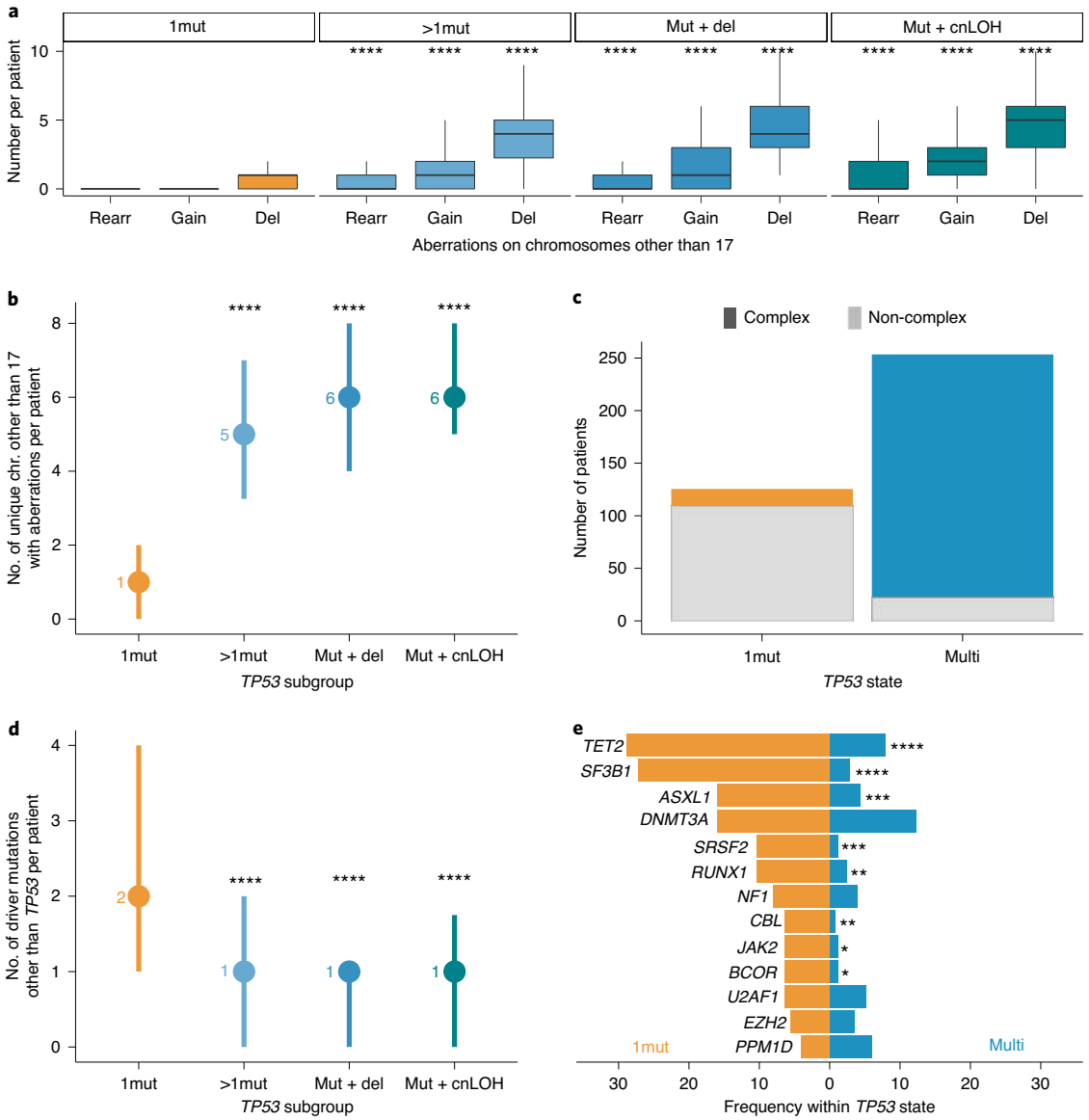

Fig. 2 | *TP53* allelic state correlates with contrasting levels of genome stability and patterns of co-mutation. a, Number of chromosomal aberrations per patient on chromosomes other than 17 across *TP53* subgroups (1mut, >1mut, mut + del and mut + cnLOH, with 125, 90, 85 and 78 patients, respectively) and types of aberrations—rearrangement (rearr), gain or deletion (del). In all boxplots, the median is indicated by the horizontal line and the first and third quartiles by the box edges. The lower and upper whiskers extend from the hinges to the smallest and largest values, respectively, no further than 1.5× interquartile range from the hinges. $^{****}P < 0.0001$, two-sided Wilcoxon rank-sum test, each compared to the same aberration within the 1mut group. **b**, Number of unique chromosomes other than 17 affected by a chromosomal aberration (rearr, gain or del) per *TP53* subgroup for 1mut ($n = 125$), >1mut ($n = 90$), mut + del ($n = 85$) and mut + cnLOH ($n = 78$). Dots represent the median across patients and lines extend from first to third quartiles. $^{****}P < 0.0001$, two-sided Wilcoxon rank-sum test, compared to the 1mut group. Wilcoxon W statistic = 9,950, 10,040 and 9,239 and $P = 2 \times 10^{-22}$, 2×10^{-28} and 1×10^{-27} for >1mut, mut + del and mut + cnLOH, respectively. **c**, Interaction between *TP53* allelic state and complex karyotype; 13% (16/125) of monoallelic *TP53* patients (1mut) had a complex karyotype and 91% (231/253) of multi-hit *TP53* patients (multi) had a complex karyotype. **d**, Number of driver mutations on genes other than *TP53* per *TP53* subgroup of 1mut ($n = 125$), >1mut ($n = 90$), mut + del ($n = 85$) and mut + cnLOH ($n = 78$). Dots represent the median across patients and lines extend from first to third quartiles. $^{****}P < 0.0001$, two-sided Wilcoxon rank-sum test compared to the 1mut group. $W = 8{,}515$, 8,499 and 7,785 and $P = 6 \times 10^{-1}$, 6×10^{-14} and 3×10^{-13} for >1mut, mut + del and mut + cnLOH, respectively **e**, Proportion of cases per *TP53* allelic state with driver mutations in genes most frequently co-mutated with *TP53*. Genes mutated in at least 5% of monoallelic ($n = 125$) or multi-hit ($n = 253$) patients are represented. $^{***}P < 0.001$, $^{**}P < 0.01$, $^{*}P < 0.05$, two-sided Fisher's exact test with Benjamini–Hochberg multiple testing correction.

The emergence of data in support of dominant negative effect (DNE)[21,22] and gain of function (GOF)[23–25] led us to test whether outcomes differed based on the nature of the underlying lesion—that is, missense, truncated or hotspot *TP53* mutations. In the multi-hit state, no differences were observed for genome instability and outcomes across mutation types (Extended Data Fig. 8 and Supplementary Fig. 17a,b), indicating that it is the loss of both wild-type copies of *TP53* that drives the dismal outcomes of *TP53*-mutated MDS patients rather than the underlying mutation types. In the monoallelic state, missense mutations in the DNA

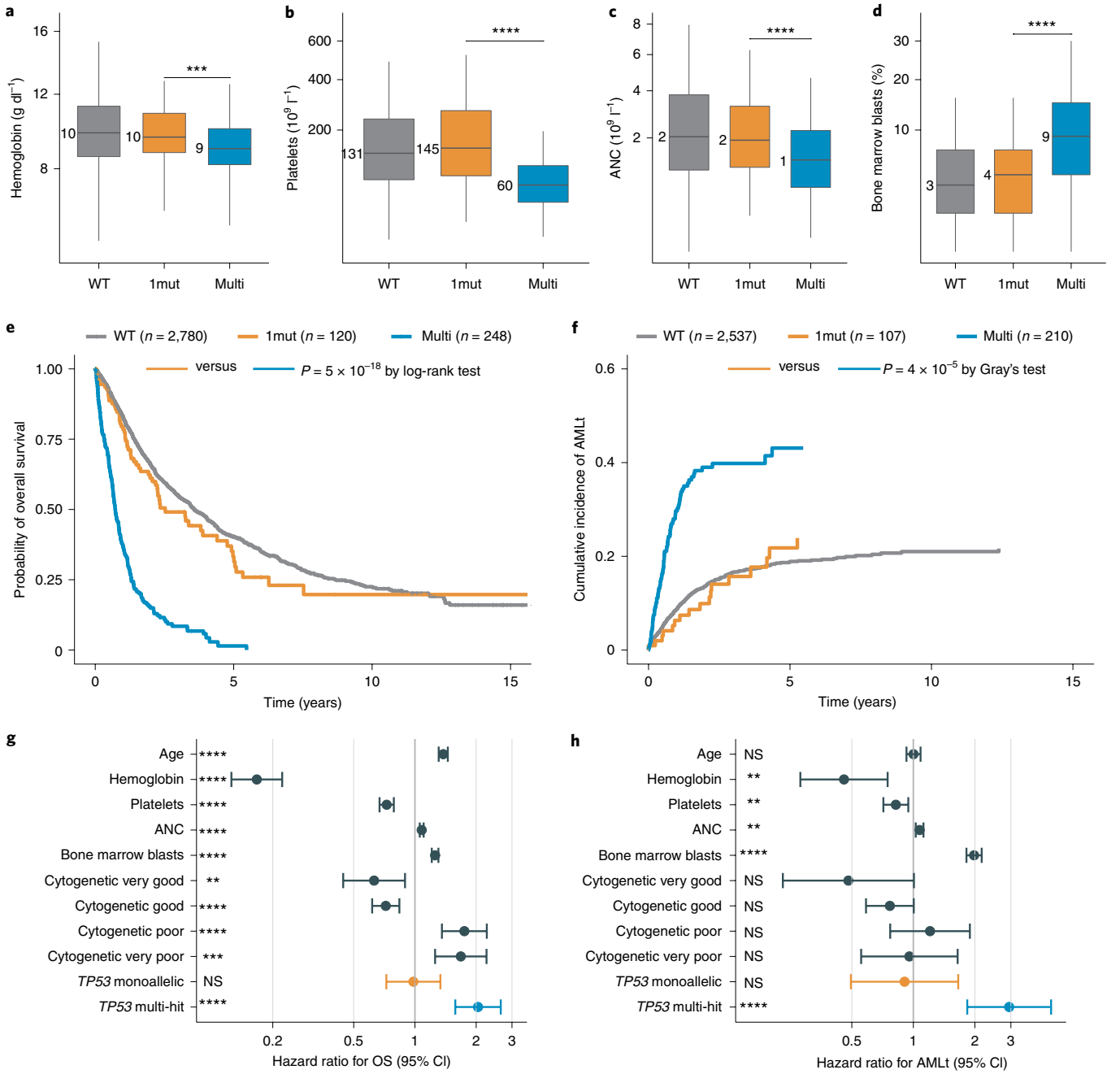

Fig. 3 | *TP53* allelic state associates with distinct clinical phenotypes and shapes patient outcomes. a–d, Boxplots indicating the levels of cytopenia, that is, hemoglobin (**a**), platelets (**b**), absolute neutrophil count (ANC) (**c**) and percentage of bone marrow blasts (**d**) per *TP53* allelic state of wild-type *TP53* (WT, $n=2{,}922$), monoallelic *TP53* (1mut, $n=125$) or multiple *TP53* hits (multi, $n=253$). In all boxplots, the median is indicated by the horizontal line and the first and third quartiles by the box edges. The lower and upper whiskers extend from the hinges to the smallest and largest values, respectively, no further than 1.5× interquartile range from the hinges. The *y*-axis values are square-rooted. $^{****}P<0.0001$, $^{***}P<0.001$, two-sided Wilcoxon rank-sum test. **e**,**f**, Kaplan–Meier probability estimates of overall survival (**e**) and cumulative AMLt (**f**) per *TP53* allelic state. The numbers of cases with outcome data per allelic state are indicated in parentheses. *P* values are derived from two-sided log-rank and Gray's tests. **g**, Results of Cox proportional hazards regression for overall survival (OS) performed on 2,719 patients with complete data for OS and with 1,290 observed deaths. Explicative variables are hemoglobin, platelets, ANC, bone marrow blasts, cytogenetic IPSS-R risk scores (very good, good, intermediate (the reference), poor and very poor) and *TP53* allelic state (monoallelic, multi-hit and wild-type is the reference). Hemoglobin, platelets, ANC and bone marrow blasts are scaled by their sample mean; age is scaled by a factor of 10; the *x*-axis is $\log_{10}$ scaled. Dots and lines represent the estimated hazard ratios and 95% confidence intervals (CI), respectively. $^{****}P<0.0001$, $^{***}P<0.001$, $^{**}P<0.01$, NS, not significant. $P>0.05$, Wald test. **h**, Results of cause-specific Cox proportional hazards regression for AMLt performed on 2,464 patients with complete data for AMLt and with 411 observed transformations. Covariates are as in **g**. Dots and lines represent estimated hazard ratios and 95% CI, respectively. $^{****}P<0.0001$, $^{**}P<0.01$, NS, not significant, $P>0.05$, Wald test.

binding domain (DBD) had no effect on patient outcomes compared to wild-type *TP53*. However, there was an increased risk of death in monoallelic patients with hotspot mutation at amino acid positions R175 and R248 (but not R273) compared to wild-type patients (HR = 2.3, 95% CI: 1.2–4.7, $P=0.02$ for R248 and HR = 3.0, 95% CI: 0.96–9.3, $P=0.06$, Wald test for R175; Supplementary

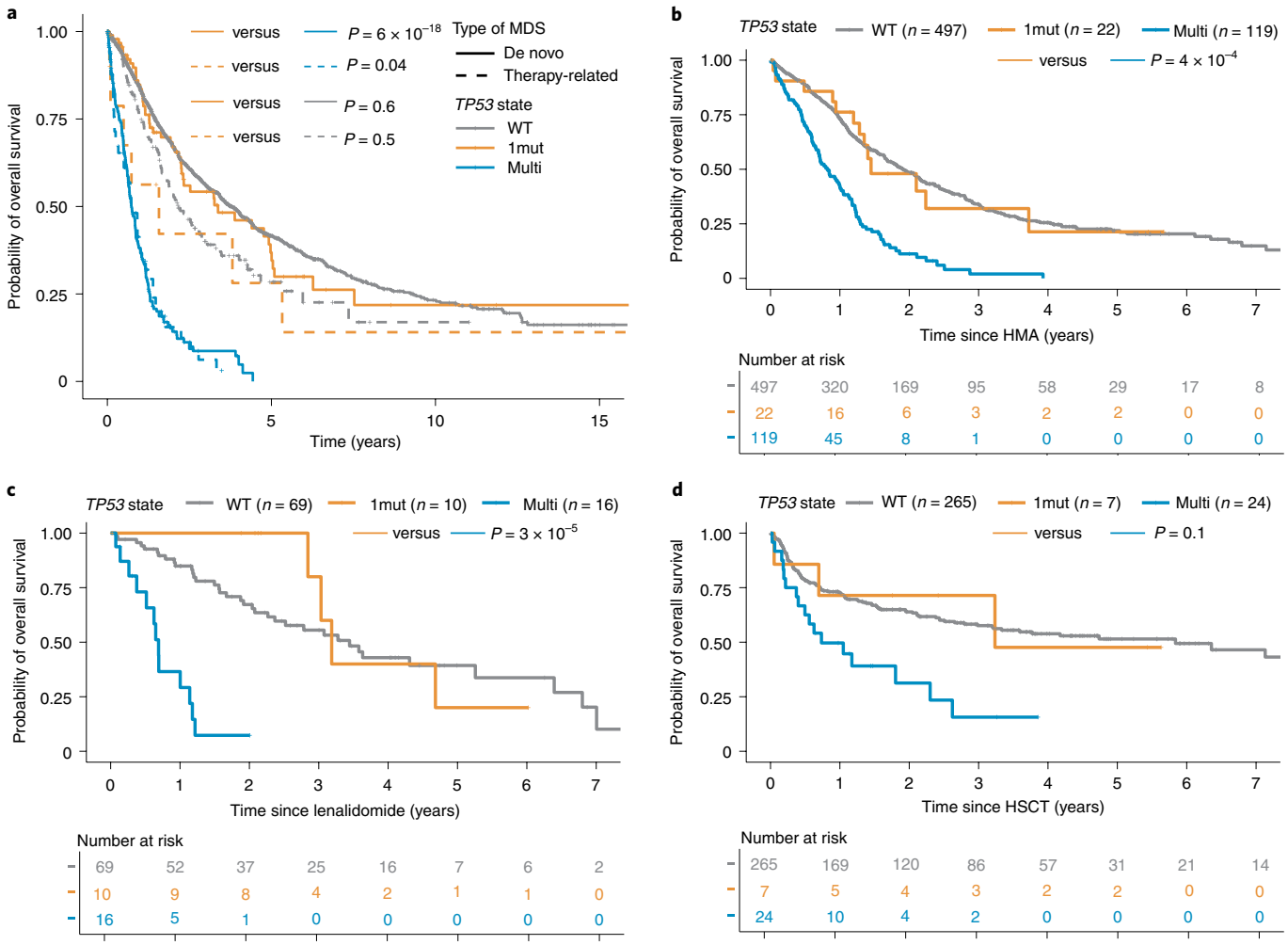

Fig. 4 | *TP53* allelic state demarcates outcomes in therapy-related MDS and on different therapies. a, Kaplan–Meier probability estimates of overall survival per *TP53* allelic state of wild-type *TP53* (WT), monoallelic *TP53* (1mut) and multiple *TP53* hits (multi), and across types of MDS, that is, de novo MDS (solid lines) or therapy-related MDS (dashed lines). Among de novo cases, 101 had a monoallelic *TP53* mutation (solid orange line), 184 were multi-hit *TP53* (solid blue line) and 2,552 were *TP53* wild-type (solid gray line). Among therapy-related cases, ten had a monoallelic *TP53* mutation (dashed orange line), 52 were multi-hit *TP53* (dashed blue line) and 162 were *TP53* wild-type (dashed gray line). Annotated *P* values are from two-sided log-rank tests. **b**–**d**, Kaplan–Meier probability estimates of overall survival (OS) following commencement of treatment with HMA (**b**) or lenalidomide for patients with del(5q) (**c**) or HSCT (**d**) per *TP53* allelic state. OS was measured from the start of treatment or HSCT to the time of death from any cause. Patients alive at the last follow-up date were censored at that time. The number of cases with OS data per *TP53* state is indicated in parentheses. Annotated *P* values are from two-sided log-rank tests.

Fig. 17c,d), consistent with either DNE[21] or GOF[25] of the hotspot mutant proteins. This suggests that DNE[21] may not be applicable to all DBD mutations, especially in the setting of MDS where exposure to genotoxic therapy is not common. Larger datasets and functional studies are warranted to further investigate the operative mechanisms of DBD mutations in MDS.

Beyond primary MDS, *TP53* mutations are enriched in therapy-related MDS (t-MDS)[6,26] and are associated with a high risk of progression to AML[5]. In t-MDS and at progression, *TP53*-mutated patients demarcate an extremely adverse prognostic group with a chemorefractory disease and <2% 5-year survival[15,16]. Our cohort included 229 t-MDS cases, with a higher proportion of *TP53*-mutated patients relative to de novo MDS (18 versus 6%, OR = 3.3, 95% CI: 2.4–4.6). *TP53*-mutated t-MDS patients more frequently had multiple hits compared to *TP53*-mutated de novo patients (84 versus 65%, OR = 2.8, 95% CI: 1.4–6.6). Comparison of genome profiles (Supplementary Fig. 18) and clinical outcomes (Fig. 4a) between allelic states reiterated observations from de novo MDS. *TP53*-mutant t-MDS is considered one of the most lethal malignancies with limited treatment options[27], yet monoallelic patients had lower risk of death compared to multi-hit patients (HR = 0.39, 95% CI: 0.15–1.0, *P* = 0.05, Wald test).

To evaluate the effect of *TP53* state in disease progression, we analyzed serial data from an independent cohort of 12 patients with MDS[28,29] (St James's University Hospital, United Kingdom) who progressed to AML with a *TP53* mutation (Supplementary Fig. 19). In 7/12 patients, multiple hits were observed at the time of MDS diagnosis, with a 4-month median to AML progression (Supplementary Fig. 19a–g). In three patients, biallelic targeting occurred during disease progression with interclonal competition and attainment of clonal dominance for the *TP53* clone (Supplementary Fig. 19h,i). The remaining two cases that progressed with a monoallelic *TP53* mutation had other high-risk mutations in either *RUNX1* and *KRAS* or *CBL* (Supplementary Fig. 19k,l), consistent with the observation from our discovery cohort that monoallelic *TP53* mutations tend to occur with several and diverse cooperating mutations (Fig. 2d,e). These data provided further evidence that biallelic alteration of *TP53* is a potent driver of disease progression, and underscore the

importance of assessing *TP53* allelic state at diagnosis and for disease surveillance.

We validated the representation of *TP53* allelic states (Supplementary Fig. 20), genome stability profiles (Supplementary Fig. 21) and differences in clinical phenotypes (Supplementary Fig. 22) in a cohort of 1,120 patients with MDS (Extended Data Fig. 2).

Last, we evaluated the implication of *TP53* allelic state in response to therapy. Recent studies have reported that *TP53* patients have poor responses to lenalidomide[8] and hematopoietic stem cell transplantation (HSCT)[6,7], as well as marked but transient responses to hypomethylating agent (HMA)[30]. We conducted an exploratory survival analysis by allelic state for patients that received HMA, lenalidomide (on the subset with deletion of 5q) and following HSCT (Extended Data Fig. 9). For HMA and lenalidomide, patients with monoallelic *TP53* mutations had evidence of longer survival compared to multi-hit patients (Fig. 4b,c). The analysis of our HSCT cohort was limited due to its size, yet we observed a trend for improved survival of monoallelic patients compared to multi-hit patients following HSCT (Fig. 4d). These observations highlight the importance of mapping *TP53* allelic states in future correlative studies of response to therapy.

In summary, we have provided a detailed characterization of *TP53* allelic state in 3,324 patients with MDS, and assessed its implication for disease biology, clinical presentation and outcomes. Two-thirds of *TP53*-mutated patients had multiple hits (more than one gene mutation, mutation and deletion, mutation and cnLOH), consistent with biallelic targeting. The remaining one-third had monoallelic mutations with one residual wild-type allele.

We have demonstrated that the multi-hit *TP53* state in MDS, not the bare presence of any *TP53* mutation, underlies established associations with genome instability, treatment resistance, disease progression and dismal outcomes. Multi-hit *TP53* identified very-high-risk patients independently of IPSS-R, co-occurring mutations and clonal representation. Surprisingly, monoallelic *TP53* patients did not differ from *TP53* wild-type patients with regard to response to therapy, overall survival and AML progression. The shift in survival for monoallelic patients with the number of co-mutations indicates diversity of disease pathogenesis and highlights the need for future prognostic models that consider a large spectrum of gene mutations.

Different evolutionary trajectories between multi-hit and monoallelic patients emerged from our data. In multi-hit state, *TP53* mutations were predominantly in the dominant clone with complex karyotypes and few other mutations, reflecting early truncal events in MDS pathogenesis. In contrast, monoallelic *TP53* mutations were frequently subclonal and co-occurred with mutations from a broad range of genes, to include genes associated with both a favorable[31] (*SF3B1*) or poor[32] (*ASXL1*, *RUNX1*, *CBL*) prognosis. A limitation of our study is that we may have missed a second hit for a small subset of cases, such as balanced rearrangement or aberrant methylation. However, the systematic differences between monoallelic and multi-hit patients across genomic and clinical metrics indicate that our definition of *TP53* allelic state delineates two biologically and clinically relevant groups. In Extended Data Fig. 10, we propose a workflow to map *TP53* allelic state in routine diagnostic practice.

Our findings imply that diagnostic and prognostic precision in MDS requires the assessment of *TP53* allelic state. We propose that biallelic *TP53* should be distinguished from monoallelic *TP53* mutations in future revisions of IPSS-R and in correlative studies of treatment response. As the most frequently mutated gene in cancer, the representation and effect of *TP53* allelic state warrant investigation across cancer indications.

Online content

Any methods, additional references, Nature Research reporting summaries, source data, extended data, supplementary information, acknowledgements, peer review information; details of author contributions and competing interests; and statements of data and code availability are available at https://doi.org/10.1038/s41591-020-1008-z.

Received: 27 November 2019; Accepted: 7 July 2020;
Published online: 03 August 2020

References

1. Kandoth, C. et al. Mutational landscape and significance across 12 major cancer types. *Nature* **502**, 333–339 (2013).
2. Zehir, A. et al. Mutational landscape of metastatic cancer revealed from prospective clinical sequencing of 10,000 patients. *Nat. Med.* **23**, 703–713 (2017).
3. Haase, D. et al. TP53 mutation status divides myelodysplastic syndromes with complex karyotypes into distinct prognostic subgroups. *Leukemia* **33**, 1747–1758 (2019).
4. Bejar, R. et al. Clinical effect of point mutations in myelodysplastic syndromes. *N. Engl. J. Med.* **364**, 2496–2506 (2011).
5. Kitagawa, M., Yoshida, S., Kuwata, T., Tanizawa, T. & Kamiyama, R. p53 expression in myeloid cells of myelodysplastic syndromes. Association with evolution of overt leukemia. *Am. J. Pathol.* **145**, 338–344 (1994).
6. Lindsley, R. C. et al. Prognostic mutations in myelodysplastic syndrome after stem-cell transplantation. *N. Engl. J. Med.* **376**, 536–547 (2017).
7. Yoshizato, T. et al. Genetic abnormalities in myelodysplasia and secondary acute myeloid leukemia: impact on outcome of stem cell transplantation. *Blood* **129**, 2347–2358 (2017).
8. Jädersten, M. et al. TP53 mutations in low-risk myelodysplastic syndromes with del(5q) predict disease progression. *J. Clin. Oncol.* **29**, 1971–1979 (2011).
9. Haferlach, T. et al. Landscape of genetic lesions in 944 patients with myelodysplastic syndromes. *Leukemia* **28**, 241–247 (2014).
10. Kastenhuber, E. R. & Lowe, S. W. Putting p53 in context. *Cell* **170**, 1062–1078 (2017).
11. Greenberg, P. L. et al. Revised international prognostic scoring system for myelodysplastic syndromes. *Blood* **120**, 2454–2465 (2012).
12. Schanz, J. et al. New comprehensive cytogenetic scoring system for primary myelodysplastic syndromes (MDS) and oligoblastic acute myeloid leukemia after MDS derived from an international database merge. *J. Clin. Oncol.* **30**, 820–829 (2012).
13. Breems, D. A. et al. Monosomal karyotype in acute myeloid leukemia: a better indicator of poor prognosis than a complex karyotype. *J. Clin. Oncol.* **26**, 4791–4797 (2008).
14. Donehower, L. A. et al. Integrated analysis of TP53 gene and pathway alterations in the cancer genome atlas. *Cell Rep.* **28**, 1370–1384 (2019).
15. Rucker, F. G. et al. TP53 alterations in acute myeloid leukemia with complex karyotype correlate with specific copy number alterations, monosomal karyotype, and dismal outcome. *Blood* **119**, 2114–2121 (2012).
16. Papaemmanuil, E. et al. Genomic classification and prognosis in acute myeloid leukemia. *N. Engl. J. Med.* **374**, 2209–2221 (2016).
17. Sallman, D. A. et al. Impact of TP53 mutation variant allele frequency on phenotype and outcomes in myelodysplastic syndromes. *Leukemia* **30**, 666–673 (2016).
18. Goel, S. et al. High prevalence and allele burden-independent prognostic importance of p53 mutations in an inner-city MDS/AML cohort. *Leukemia* **30**, 1793–1795 (2016).
19. Montalban-Bravo, G. et al. Genomic context and TP53 allele frequency define clinical outcomes in TP53-mutated myelodysplastic syndromes. *Blood Adv.* **4**, 482–495 (2020).
20. Lausen, B. & Schumacher, M. Maximally selected rank statistics. *Biometrics* **48**, 73–85 (1992).
21. Boettcher, S. et al. A dominant-negative effect drives selection of TP53 missense mutations in myeloid malignancies. *Science* **365**, 599–604 (2019).
22. Levine, A. J. The many faces of p53: something for everyone. *J. Mol. Cell Biol.* **11**, 524–530 (2019).
23. Lang, G. A. et al. Gain of function of a p53 hot spot mutation in a mouse model of li-Fraumeni syndrome. *Cell* **119**, 861–872 (2004).
24. Olive, K. P. et al. Mutant p53 gain of function in two mouse models of Li-Fraumeni syndrome. *Cell* **119**, 847–860 (2004).
25. Loizou, E. et al. A gain-of-function p53-mutant oncogene promotes cell fate plasticity and myeloid leukemia through the pluripotency factor FOXH1. *Cancer Discov.* **9**, 962–979 (2019).
26. Wong, T. N. et al. Role of TP53 mutations in the origin and evolution of therapy-related acute myeloid leukaemia. *Nature* **518**, 552–555 (2015).
27. Platzbecker, U. Treatment of MDS. *Blood* **133**, 1096–1107 (2019).
28. Roman, E. et al. Myeloid malignancies in the real-world: occurrence, progression and survival in the UK's population-based Haematological Malignancy Research Network 2004–15. *Cancer Epidemiol.* **42**, 186–198 (2016).

29. Smith, A. et al. Cohort profile: the Haematological Malignancy Research Network (HMRN); a UK population-based patient cohort. *Int. J. Epidemiol.* **47**, 700–700g (2018).
30. Welch, J. S. et al. TP53 and decitabine in acute myeloid leukemia and myelodysplastic syndromes. *N. Engl. J. Med.* **375**, 2023–2036 (2016).
31. Malcovati, L. et al. Clinical significance of SF3B1 mutations in myelodysplastic syndromes and myelodysplastic/myeloproliferative neoplasms. *Blood* **118**, 6239–6246 (2011).
32. Papaemmanuil, E. et al. Clinical and biological implications of driver mutations in myelodysplastic syndromes. *Blood* **122**, 3616–3627 (2013). quiz 3699.

[1]Computational Oncology Service, Department of Epidemiology & Biostatistics, Memorial Sloan Kettering Cancer Center, New York, NY, USA. [2]Center for Hematologic Malignancies, Memorial Sloan Kettering Cancer Center, New York, NY, USA. [3]Department of Pathology and Tumor Biology, Kyoto University, Kyoto, Japan. [4]Department of Pathology, Massachusetts General Hospital, Boston, MA, USA. [5]Department of Epidemiology & Biostatistics, Memorial Sloan Kettering Cancer Center, New York, NY, USA. [6], Vienna, Austria. [7]Department of Molecular Medicine, University of Pavia, Pavia, Italy. [8]Department of Hematology, IRCCS Fondazione Policlinico S. Matteo, Pavia, Italy. [9]MDS Group, Institut de Recerca Contra la Leucèmia Josep Carreras, Barcelona, Spain. [10]Haematological Malignancy Diagnostic Service, St James's University Hospital, Leeds, UK. [11]Clinics of Hematology and Medical Oncology, University Medical Center, Göttingen, Germany. [12]Department of Medicine Huddinge, Center for Hematology and Regenerative Medicine, Karolinska Institutet, Karolinska University Hospital, Stockholm, Sweden. [13]Department of Hematology, Oncology and Clinical Immunology, Heinrich Heine University, Düsseldorf, Germany. [14]Department of Pathology, Memorial Sloan Kettering Cancer Center, New York, NY, USA. [15]Department of Hematology, VU University Medical Center Amsterdam, Amsterdam, the Netherlands. [16]Department of Hematology, Assistance Publique-Hôpitaux de Paris, Hôpital Cochin and Université de Paris, Université Paris Descartes, Paris, France. [17]Department of Biomedical and Neuromotor Sciences, University of Bologna, Bologna, Italy. [18]Department of Hematology, Hemostasis, Oncology and Stem Cell Transplantation Hannover Medical School, Hannover, Germany. [19]Drug Research and Development Center, Federal University of Ceara, Ceara, Brazil. [20]MDS Unit, Hematology, AOU Careggi, University of Florence, Florence, Italy. [21]Department of Hematology, Democritus University of Thrace Medical School, Alexandroupolis, Greece. [22]Radcliffe Department of Medicine, University of Oxford and Oxford BRC Haematology Theme, Oxford, UK. [23]Oncology-Hematology Center, Hospital Israelita Albert Einstein, São Paulo, Brazil. [24]Department of Hematology, Gifu Municipal Hospital, Gifu, Japan. [25]Department of Hematology, Kobe City Medical Center General Hospital, Kobe, Japan. [26]Department of Hematology, Gifu University Graduate School of Medicine, Gifu, Japan. [27]Department of Hematology and Oncology, Graduate School of Medicine, Kyoto University, Kyoto, Japan. [28]Department of Hematology, Chugoku Central Hospital, Fukuyama, Japan. [29]Department of Medicine, Chulalongkorn University, King Chulalongkorn Memorial Hospital, Bangkok, Thailand. [30]Lab. Medicine and Pathology, Hematology/Oncology, University of Rochester Medical Center, Rochester, NY, USA. [31]Department of Medicine, Memorial Sloan Kettering Cancer Center, New York, NY, USA. [32]Department of Medicine, Vanderbilt-Ingram Cancer Center, Vanderbilt University School of Medicine, Nashville, TN, USA. [33]Department of Genomics, Institute of Hematology and Blood Transfusion, Prague, Czech Republic. [34]Department of Hematology, Hospital Universitario y Politécnico La Fe, Valencia, Spain. [35]CIBERONC, Instituto de Salud Carlos III, Madrid, Spain. [36]Department of Hematology, Hôpital St Louis and Paris University, Paris, France. [37]Cancer Center, Humanitas Research Hospital & Humanitas University, Milan, Italy. [38]Department of Health Sciences, University of York, York, UK. [39]Integrated Genomics Operation, Memorial Sloan Kettering Cancer Center, New York, NY, USA. [40]Department of Data Sciences, Dana-Farber Cancer Institute, Boston, MA, USA. [41]Medical Clinic and Policlinic 1, Hematology and Cellular Therapy, University of Leipzig, Leipzig, Germany. [42]Department of Internal Medicine I, Division of Hematology and Hemostaseology and Ludwig Boltzmann Institute for Hematology and Oncology, Medical University of Vienna, Vienna, Austria. [43]Department of Hematology, Faculty of Medicine, University of Tsukuba, Tsukuba, Japan. [44]Department of Hematology, Atomic Bomb Disease Institute, Nagasaki University, Nagasaki, Japan. [45]Institute of Hematology, S. Orsola-Malpighi University Hospital, Bologna, Italy. [46]MDS Cooperative Group GROM-L, Department of Biomedicine and Prevention, Tor Vergata University, Rome, Italy. [47]Chang Gung Memorial Hospital at Linkou, Chang Gung University, Taoyuan City, Taiwan. [48]Laboratory Hematology, Department LABGK, Radboud University Medical Centre, Nijmegen, the Netherlands. [49]Department of Hematology and Genetics Unit, University Hospital La Fe, Valencia, Spain. [50]Japanese Data Center for Hematopoietic Cell Transplantation, Nagoya, Japan. [51]Department of Medical Oncology and Howard Hughes Medical Institute, Dana-Farber Cancer Center, Boston, MA, USA. [52]UC San Diego Moores Cancer Center, La Jolla, CA, USA. [53]Stanford University Cancer Institute, Stanford, CA, USA. [54]These authors jointly supervised this work: Seishi Ogawa, Elli Papaemmanuil. ✉e-mail: papaemme@mskcc.org

Methods

Patient samples. The International Working Group for Prognosis in MDS (IWG-PM) cohort originated from 24 MDS centers (Supplementary Table 1) that contributed peridiagnosis MDS, myelodysplastic/myeloproliferative neoplasms (MDS/MPN) and AML/AML with myelodysplasia-related changes (AML-MRC) patient samples to the study. Following quality control (Supplementary Fig. 1), 3,324 samples were included in the study (Extended Data Fig. 1). The source for genomic DNA was either bone marrow or peripheral blood mononuclear cells. The median time from diagnosis to sampling was 0 d (first quartile, 0 d; third quartile, 113 d). The validation cohort consisted of 1,120 samples from the Japanese MDS consortium (Extended Data Fig. 2). Samples were obtained with informed consent in accordance with the Declaration of Helsinki and appropriate Ethics Committee approval from each IWG-PM partner institution.

Clinical data. Diagnostic clinical variables were provided by the contributing centers and curated to ensure uniformity of metrics across centers and countries. Clinical variables included (1) sex; (2) age at diagnosis; (3) WHO disease subtype; (4) MDS type (de novo, secondary or therapy-related); (5) differential blood counts to include hemoglobin, platelets, white blood cells, neutrophils and monocytes; (6) percentage of bone marrow and peripheral blood blasts; (7) cytogenetic data; and (8) risk score as per IPSS-R[11]. Clinical outcomes included the time of death from any cause or last follow-up from sample collection, and the time of AML transformation or last follow-up from sample collection.

Cytogenetic data. Conventional G-banding analysis (CBA) data were available for 2,931 patients, and karyotypes were described in accordance with the International System for Human Cytogenetic Nomenclature[33]. CBA data were risk stratified according to the IPSS-R guidelines[12] using both algorithmic and manual classification by an expert panel of cytogeneticists.

WHO subtypes. Contributing centers provided the vast majority of disease classification as per WHO 2008. A pathology review was performed uniformly on the entire cohort, to ensure concordance between disease classification and diagnostic variables and to update the classification as per WHO 2016. The cohort was representative of all MDS WHO subtypes and included 563 (17%) MDS/MPN and 167 (5%) AML/AML-MRC samples (Extended Data Fig. 1).

IPSS-R risk scores. IPSS-R risk scores were uniformly calculated based on both IPSS-R cytogenetic risk scores and values for hemoglobin, platelets, absolute neutrophil count (ANC) and percentage of bone marrow blasts. All IPSS-R risk groups were represented (Extended Data Fig. 1).

Targeted sequencing. *Panel design.* The panel used for targeted sequencing included genes recurrently mutated in MDS, as well as 1,118 genome-wide single-nucleotide polymorphism (SNP) probes for copy number analysis, with on average one SNP probe every 3 Mb. Bait tiling was conducted at 2×. Baits were designed to span all exonic regions of *TP53* across all transcripts, as described in RefSeq (NM_001276761, NM_001276695, NM_001126114, NM_00112611), and included 20-base pair (bp) intronic flanking regions.

Library preparation and sequencing. For library construction, 11–800 ng of genomic DNA was used with the KAPA Hyper Prep Kit (Kapa Biosystems, no. KK8504) with 7–12 cycles of PCR. After sample barcoding, 10–1,610 ng of each library was pooled and captured by hybridization. Captured pools were sequenced with paired-end Illumina HiSeq at a median coverage of 730× per sample (range, 127–2,480×). Read length was either 100 or 125 bp.

We also sequenced 48 samples on the panel with the same sequencing conditions used for tumor samples, from the blood of young individuals who did not have hematological disease, to help further filtering of sequencing artifacts and germline SNPs.

Sequencing was performed in an unmatched setting—that is, without a matched normal tissue control per patient—so that variants had to be curated accordingly (see Variant calling and filtering for artifacts and germline variants).

Alignment. Raw sequence data were aligned to the human genome (NCBI build 37) using BWA[34] v.0.7.17. PCR duplicate reads were marked with Picard tools (https://broadinstitute.github.io/picard/) v.2.18.2. For alignment, we used the pcap-core dockerized pipeline v.4.2.1 available at https://github.com/cancerit/PCAP-core.

Sample quality control. Quality control (QC) of fastq and bam data was performed with FastQC (http://www.bioinformatics.babraham.ac.uk/projects/fastqc/) v.0.11.5 and Picard tools, respectively.

In addition, a number of downstream QC steps were performed, including:

- Fingerprinting—that is, evaluation of the similarity between all pairs of samples, based on the respective genotype on 1,118 SNPs. Duplicate samples were excluded from the study.
- Evaluation of concordance between patient sex from the clinical data and coverage on the sex chromosomes. Discordant cases were discussed with the contributing centers to rule out patients with Klinefelter syndrome and filter out erroneous samples appropriately.
- Evaluation of concordance between CBA data and NGS-derived copy number profiles (see Copy number and LOH analysis). A typical discordant case is one where CBA reports a given deletion or gain in a high number of metaphases and the NGS profile clearly shows other abnormalities not reported by CBA. All discordant cases were reviewed by a panel of experts through the IWG cytogenetic committee.

Finally, samples that passed QC but were found not to be treatment naive—that is, the patient received disease-modifying treatment before sample collection—were excluded from the study. Supplementary Fig. 1 summarizes the QC workflow.

Variant calling and filtering for artifacts and germline variants. Variants were derived from a combination of variant callers. For single nucleotide variants (SNVs), we used CaVEMan (http://cancerit.github.io/CaVEMan/) v.1.7.4, Mutect[35] v.4.0.1.2 and Strelka[36] v.2.9.1. For small insertions and deletions (indels), we used Pindel[37] v.1.5.4, Mutect v.4.0.1.2 and Strelka v.2.9.1. VAFs were uniformly reported across all called variants using the vafCorrect realignment procedure available at https://github.com/cancerit/vafCorrect. All called variants were annotated with VAGrENT (https://github.com/cancerit/VAGrENT) v.3.3.0 and Ensembl-VEP (https://github.com/Ensembl/ensembl-vep) with Ensembl v.91 and VEP release 94.5.

Artifact variants were filtered out based on:

- Off-target variants—that is, variants called outside of the panel target regions were excluded
- Variants with VAF < 2%, <20 total reads or <5 mutant supporting reads were excluded
- The number of callers calling a given variant and the combination of filters (flags) from the triple callers; more specifically:
  - For SNVs, variants called by CaVEMan with >2 CaVEMan flags (from the DTH, RP, MN, PT, MQ, SR, TI, SRP, VUM, SE list) were excluded. Variants called only by Strelka and Mutect (but not CaVEMan) were filtered out if they had >0 flags or if the dirprop metric (ratio of number of reads on each strand) was <0.44. Variants called only by Mutect (but not by CaVEMan or Strelka) were filtered out if they had >0 flags or if dirprop was <0.44 or VAF < 5%.
  - For indels, variants called by all three callers (Pindel, Mutect and Strelka) were excluded if they had >3 flags. Variants called by only two callers were excluded if they had >2 flags. Variants called only by Pindel were filtered out if they had >1 flag or <2 mutant reads on one strand. Variants called only by Mutect were filtered out if they had >0 flags or <2 mutant reads on one strand.
- Recurrence and VAF distribution of the called variants on a panel of 48 normal samples

After prefiltering of artifactual variants, germline SNPs were filtered out by consideration of:

- VAF density of variants consistent with germline SNP
- Presence in the Genome Aggregation Database (gnomAD)[38]. More specifically, variants with a population-based allele frequency (VEP_gnomAD_AF) >0.001 were excluded (with the exception of a few variants in *SH2B3* involved in familial thrombocythemia). Variants with a maximum allele frequency across the gnomAD populations (VEP_MAX_AF) >0.01 were excluded (with the exception of *ASXL1* amino acid position G646, which requires specific rescue).
- Recurrence in a panel of normals

All remaining probable somatic variants after the above-mentioned filtering were manually inspected with Integrative Genomics Viewer[39] to rule out residual artifacts.

Variant annotation for putative oncogenicity. From the list of probable somatic variants, putative oncogenic variants were distinguished from variants of unknown significance based on:

- Recurrence in the Catalog Of Somatic Mutations in Cancer (COSMIC)[40], in myeloid disease samples registered in cBioPortal[40,41] and in the study dataset
- Presence in pan-cancer hotspot databases[42,43]
- Annotation in the human variation database ClinVar[44]
- Annotation in the precision oncology knowledge database OncoKB[45]
- Recurrence with somatic presentation in a set of in-house data derived from >6,000 myeloid neoplasms[16,32,46]
- The inferred consequence of a mutation where nonsense mutations, splice site mutations and frameshift indels were considered oncogenic in tumor suppressor genes (from COSMIC Cancer Census Genes or OncoKB Cancer Gene List)

For annotation of oncogenicity of *TP53* variants we additionally considered:

- Functional annotation in the International Agency for Research on Cancer (IARC) *TP53* database[47]
- Functional classification *TP53* prediction scores using PHANTM[48]

Supplementary Fig. 5 illustrates the rationale and results of the annotation of *TP53* variants for putative oncogenicity.

Copy number and LOH analysis. In addition to CBA, we assessed chromosomal alterations based on NGS sequencing data using CNACS[7]. CNACS enables the detection of arm-level and focal copy number changes as well as regions of cnLOH. CNACS has been optimized to run in the unmatch setting and uses a panel of normals for calibration.

Supplementary Fig. 2 provides examples of characterization of allelic imbalances (gains, deletions and regions of cnLOH) using CNACS, with concordant copy number change findings between CBA and CNACS, focal deletions exclusively detected with CNACS and, as expected, regions of cnLOH detected only by CNACS. For genome-wide analysis, we considered CNACS segments >3 Mb with minor allele frequency <45% (when 50% represents no allelic imbalance). Supplementary Fig. 4 provides examples of characterization of allelic imbalances by CNACS and SNP arrays on 21 selected samples, with highly concordant findings between the two assays.

In addition to CNACS, we also ran CNVkit[49] v.0.9.6 on the study cohort. Because CNVkit does not infer allele-specific copy numbers, it does not allow marking regions of cnLOH but it estimates copy number changes. The integration of two copy number tools increased the specificity and sensitivity of copy number calling.

For 2,931 patients with CBA data we performed a detailed comparison of CBA- and NGS-derived copy number results (Supplementary Fig. 3), which showed highly concordant findings. Along with the annotation of regions of cnLOH, we supplemented the presence of copy number changes on patients when it was clear on NGS results but missed by CBA (for example, focal deletions). In 393 patients with missing CBA data, we used the NGS results to fully annotate copy number changes. Because our NGS assay did not allow the detection of translocations, inversions, whole-genome amplification and the presence of marker or ring chromosomes, those specific alterations were statistically imputed from other molecular markers on these 393 patients.

Complex karyotype. Among 2,931 patients with CBA data, 310 had a complex karyotype identified by CBA, where complex karyotype was defined as three or more independent chromosomal abnormalities. Among those 2,931 patients, NGS results helped to identify complex karyotypes in an additional 15 patients. Among the 393 cases with missing CBA data, 13 had a complex karyotype according to NGS copy number profiles (Supplementary Fig. 3c). Overall 329 patients had a complex karyotype, representing 10% of the study cohort.

Statistics. All statistical analyses were conducted using the R statistical platform (https://www.r-project.org/) v.3.6.1. Fisher's exact test and Wilcoxon rank-sum test were used to compare categorical and continuous variables. All statistical tests were two-sided. Benjamini–Hochberg multiple testing correction was applied when appropriate.

Overall survival. Overall survival was measured from the time of sample collection to the time of death from any cause. Patients alive at the last follow-up date were censored at that time. Survival probabilities over time were estimated using Kaplan–Meier methodology, and comparisons of survival across subgroups were conducted using the two-sided log-rank test. Kaplan–Meier estimates were computed using the R package survival.

Multivariable models of overall survival were performed with Cox proportional hazards regression, using the R package coxph. Hazard ratios and 95% CIs were reported for covariates, along with *P* values from the Wald test. Covariates included in the multivariable model of overall survival were age, hemoglobin, platelets, ANC, bone marrow blasts, cytogenetic risk group and *TP53* allelic state. Hemoglobin, platelets, ANC and bone marrow blasts were treated as continuous variables and were scaled by their sample mean. Age was treated as a continuous variable and was scaled by a factor of ten. Cytogenetic risk group was treated as a categorical variable, with the intermediate risk group as the reference group. *TP53* allelic state was treated as a categorical variable, with the wild-type state as the reference group relative to monoallelic and multi-hit groups. Those covariates correspond to all covariates included in the age-adjusted IPPS-R model along the *TP53* allelic state.

AML transformation (AMLt). In univariate analysis of AMLt, time to AMLt was measured from the time of sample collection to the time of transformation, with death without transformation treated as a competing risk. Patients alive without AMLt at the last contact date were censored at that time. Cumulative incidence functions were used to estimate the incidence of AMLt using the R package cmprsk, and comparisons of cumulative incidence function across subgroups were conducted using the two-sided Gray's test.

Multivariable models of AMLt were performed using cause-specific Cox proportional hazards regressions, where patients who did not transform but died were censored at the time of death. Hazard ratios and 95% CIs were reported for the covariates, along with *P* values from the Wald test. Covariates included in the multivariable model of AMLt were the same as those in the model of overall survival described above.

Reporting Summary. Further information on research design is available in the Nature Research Reporting Summary linked to this article.

Data availability

Clinical, copy number and mutation data are available at https://github.com/papaemmelab/MDS-TP53-state. The data underlying Figs. 1–4 are provided as Source Data.

Databases used in the study are gnomAD (https://gnomad.broadinstitute.org), COSMIC (https://cancer.sanger.ac.uk/cosmic), cBioPortal for Cancer Genomics (https://www.cbioportal.org), OncoKB Precision Oncology Knowledge Base (https://www.oncokb.org), ClinVar (https://www.ncbi.nlm.nih.gov/clinvar) and the IARC TP53 Database (https://p53.iarc.fr).

Code availability

The NGS-based, allele-specific copy number algorithm CNACS[7] is available as a python toil workflow engine at https://github.com/papaemmelab/toil_cnacs, where release v.0.2.0 was used in this study. Source code to reproduce figures from the manuscript is available at https://github.com/papaemmelab/MDS-TP53-state.

References

33. International Standing Committee on Human Cytogenetic Nomenclature. *ISCN 2013: An International System for Human Cytogenetic Nomenclature* (Karger, 2013).
34. Li, H. & Durbin, R. Fast and accurate long-read alignment with Burrows–Wheeler transform. *Bioinformatics* **26**, 589–595 (2010).
35. Cibulskis, K. et al. Sensitive detection of somatic point mutations in impure and heterogeneous cancer samples. *Nat. Biotechnol.* **31**, 213–219 (2013).
36. Saunders, C. T. et al. Strelka: accurate somatic small-variant calling from sequenced tumor-normal sample pairs. *Bioinformatics* **28**, 1811–1817 (2012).
37. Ye, K., Schulz, M. H., Long, Q., Apweiler, R. & Ning, Z. Pindel: a pattern growth approach to detect break points of large deletions and medium sized insertions from paired-end short reads. *Bioinformatics* **25**, 2865–2871 (2009).
38. Karczewski, K. J. et al. Variation across 141,456 human exomes and genomes reveals the spectrum of loss-of-function intolerance across human protein-coding genes. *Nature* **581**, 434–443 (2020).
39. Thorvaldsdóttir, H., Robinson, J. T. & Mesirov, J. P. Integrative Genomics Viewer (IGV): high-performance genomics data visualization and exploration. *Brief. Bioinformatics* **14**, 178–192 (2013).
40. Tate, J. G. et al. COSMIC: the catalogue of somatic mutations in cancer. *Nucleic Acids Res.* **47**, D941–D947 (2019).
41. Cerami, E. et al. The cBio cancer genomics portal: an open platform for exploring multidimensional cancer genomics data. *Cancer Discov.* **2**, 401–404 (2012).
42. Chang, M. T. et al. Identifying recurrent mutations in cancer reveals widespread lineage diversity and mutational specificity. *Nat. Biotechnol.* **34**, 155–163 (2016).
43. Chang, M. T. et al. Accelerating discovery of functional mutant alleles in cancer. *Cancer Discov.* **8**, 174–183 (2018).
44. Landrum, M. J. et al. ClinVar: public archive of relationships among sequence variation and human phenotype. *Nucleic Acids Res.* **42**, D980–D985 (2014).
45. Chakravarty, D. et al. OncoKB: a precision oncology knowledge base. *JCO Precis. Oncol.* **2017**, 10.1200 (2017).
46. Grinfeld, J. et al. Classification and personalized prognosis in myeloproliferative neoplasms. *N. Engl. J. Med.* **379**, 1416–1430 (2018).
47. Bouaoun, L. et al. TP53 variations in human cancers: new lessons from the iarc tp53 database and genomics data. *Hum. Mutat.* **37**, 865–876 (2016).
48. Giacomelli, A. O. et al. Mutational processes shape the landscape of TP53 mutations in human cancer. *Nat. Genet.* **50**, 1381–1387 (2018).
49. Talevich, E., Shain, A. H., Botton, T. & Bastian, B. C. CNVkit: genome-wide copy number detection and visualization from targeted DNA sequencing. *PLoS Comput. Biol.* **12**, e1004873 (2016).

Acknowledgements

This work was supported in part by grants from the Celgene Corporation through the MDS Foundation. It was also supported by grants-in-aid from the Japan Agency for Medical Research and Development (AMED) (JP19cm0106501, JP19ck0106250 and 15H05909 (S.O.) and JP18ck0106353 (Y.N.)), from the Japan Society for the Promotion of Science (JSPS) (KAKEN JP26221308, JP19H05656 (S.O.)) and from the Ministry of Education, Culture, Sports, Science and Technology (hp160219 (S.O.)). J.B. and A.P. acknowledge funding from Blood Cancer UK (grant 13042). P.V. was supported by the Austrian Science Fund (grant F4704-B20). M.Y.F. was supported by Italian MIUR-PRIN grants. L.M. was supported by the Associazione Italiana per la Ricerca sul Cancro (AIRC, Milan, Italy) 5 per Mille project (21267 and IG 20125). M.T.V. was supported by AIRC 5 per Mille project (21267). M.T.V. recruited patients through the GROM-L clinical network. E.B. was supported by the Francois Wallace Monahan Fellowship and an EvansMDS Young Investigator award. E.P. is a Josie Robertson Investigator and is supported by the European Hematology Association, the American Society of Hematology, Gabrielle's Angels Foundation, V Foundation and The Geoffrey Beene Foundation. We thank T. Iraca for logistical support.

Author contributions

E.B. and E.P. designed the study. E.B. and Y.N. performed statistical analysis. S.D. and E.P. supervised statistical analysis. L.M., B.L.E., R.B., P.L.G., M. Cazzola, E.H.-L., S.O. and E.P. supervised research. P.L.G. and E.P. coordinated the study. L.M., F.S., C.A.C., M. Creignou, U.G., A.A.L., M.J., M.T., O.K., M.Y.F., F.T., R.F.P., V.S., I.K., J.B., F.P.S.S., S.K., T.I., T.H., A.T.-K., T.K., C.P., V.M.K., M.R.S., M.B., C.G., L.P., L.A., M.G.D.P., P.F., A.P., U.P., M.H., P.V., S.C., Y.M., C.F., M.T.V., L.-Y.S., M.F., J.H.J., J.C., Y.A., N.G., M. Cazzola, E.H.-L. and S.O. provided clinical data and DNA specimens. E.B., Y.W., M.P. and E.P. coordinated sample acquisition. A.V. and K.V. performed sample preparation and sequencing. E.B., R.P.H., H.T. and M. Creignou curated clinical data. R.P.H. and J.M.B. performed pathology review. E.B. and H.T. processed cytogenetic data. F.S., D.H. and J.S. performed cytogenetic review. E.B., Y.N., J.S.M.-M., T.Y., A.S. and G.G. performed bioinformatic analysis. J.S.M.-M., M.F.L., J.E.A. and J.Z. supported sequence data pipelines. Y.S. and R.S. developed copy number algorithm CNACS. M.F.L. generated copy number profiles. Y.Z. performed SNP array analysis. E.B. and Y.N. prepared figures and tables. E.B., S.O. and E.P. wrote the manuscript. All authors reviewed the manuscript during its preparation.

Competing interests

The authors declare the following competing interests. U.G. has received honoraria from Celgene, Novartis, Amgen, Janssen, Roche and Jazz and research funding from Celgene and Novartis. C.A.C. has received research funding from Celgene. A.A.L. is in advisory boards of Celgene, Amgen, Roche, Novartis and Alexion and has received research funding from Celgene. F.T. is on the advisory boards of Jazz, Pfizzer and Abbvie and has received research funding from Celgene. I.K. is on the advisory board of Genesis Pharma and has received research funding from Celgene and Janssen Hellas. F.P.S.S. has received honoraria from Janssen-Cilag, Bristol-Myers-Squibb, Novartis, Amgen, Abbvie and Pfizer, is on the advisory boards of Novartis, Amgen and Abbvie and has received research funding from Novartis. A.T.-K. has received honoraria from Novartis, Bristol-Myers-Squibb and MSD and has received research funding from Celgene, Ono Pharmaceutical and Cognano. T.K. has received research funding from Bristol-Myers-Squibb, Otsuka Pharmaceutical, Kyowa Kirin, MSD, Astellas Pharmaceutical, Nippon Shinyaku, Novartis Pharmaceutical, Sumitomo Dainippon Pharmaceutical, Janssen Pharmaceutical, Celgene, SymBio Pharmaceutical, Taiho Pharmaceutical, Tejin, Sanofi K.K. and Celltrion. M.R.S. is on the advisory boards of Abbvie, Astex, Celgene, Karyopharm, Selvita and TG Therapeutic, has equity in Karyopharm and has received research funding from Astex, Incyte, Sunesis, Takeda and TG Therapeutics. G.S. is on the advisory boards of AbbVie, Amgen, Astellas, Böehringer-Ingelheim, Celgene, Helsinn Healthcare, Hoffmann-La Roche, Janssen-Cilag, Novartis and Onconova and has received research funding from Celgene, Hoffmann-La Roche, Janssen-Cilag and Novartis. L.A. is on the advisory boards of Abbvie, Astex, Celgene and Novartis and has received research funding from Celgene. D.S.N. has equity in Madrigal Phamaceuticals and has received research funding from Celgene and Pharmacyclics. K.L.B. has received research funding from GRAIL. M.H. has received honoraria from Novartis, Pfizer and PriME Oncology, is on the advisory boards of Abbvie, Bayer Pharma, Daiichi Sankyo, Novartis and Pfizer and has received institutional research funding from Astellas, Bayer Pharma, BergenBio, Daiichi Sankyo, Karyopharm, Novartis, Pfizer and Roche. P.V. has received honoraria and research funding from Celgene. S.C. has received research funding from Kyowa Kirin, Chugai Pharmaceutical, Takeda Pharmaceutical, Astellas Pharmaceutical, Sanofi KK and Ono Pharmaceutical. Y.M. has received honoraria from Ohtsuka, Novartis, Nippon Shinyaku, Dainippon-Sumitomo and Kyowa Kirin and research funding from Chugai. C.F. is on the advisory boards of, and has received honoraria from, Celgene, Novartis and Janssen and has received research funding from Celgene. M.T.V. is on the advisory board of Celgene, has received honoraria from Celgene and Novartis and has received research funding from Celgene. Y.A. has received honoraria from Mochida, Meiji, Chugai and Kyowa Kirin. N.G. is on the advisory board of, and has received honoraria from, Novartis and has received research funding from Alexion. B.L.E. has received research funding from Celgene and Deerfield. R.B. is on the advisory boards of Celgene, AbbVie, Astex, NeoGenomics and Daiichi Sankyo and has received research funding from Celgene and Takeda. E.H.-L. has received research funding from Celgene. E.B. has received research funding from Celgene. E.P. has received research funding from Celgene and has served on scientific advisory boards for Novartis. E.P. is the founder and CEO of Isabl, a company offering analytics for cancer whole-genome sequencing data.

Additional information

Extended data is available for this paper at https://doi.org/10.1038/s41591-020-1008-z.

Supplementary information is available for this paper at https://doi.org/10.1038/s41591-020-1008-z.

Correspondence and requests for materials should be addressed to E.P.

Peer review information Javier Carmona was the primary editor on this article, and managed its editorial process and peer review in collaboration with the rest of the editorial team.

Reprints and permissions information is available at www.nature.com/reprints.

IWG-MDS cohort (N=3324)		
Characteristic	**No. of cases (%)**	**Median (1Q - 3Q)**
Gender		
Male	2005 (60%)	-
Female	1319 (40%)	-
Age at diagnosis	-	71 (63 - 78)
Missing data	85 (2.6%)	-
Type of MDS		
De-novo	2855 (86%)	-
Therapy-related	229 (7%)	-
Secondary	51 (1%)	-
Missing data	189 (6%)	-
WHO 2016 classification		
MDS		
MDS-del5q	142 (4.3%)	-
MDS-SLD/MLD	914 (27.5%)	-
MDS-RS-SLD/MLD	460 (13.8%)	-
MDS-EB1	451 (13.6%)	-
MDS-EB2	429 (12.9%)	-
MDS-U	92 (2.8%)	-
AML		
AML-MRC	103 (3%)	-
AML[#]	64 (2%)	-
MDS/MPN		
CMML	425 (12.8%)	-
aCML	46 (1.4%)	-
MDS/MPN-U	50 (1.5%)	-
MDS/MPN-RS-T	42 (1.3%)	-
Other	11 (0.3%)	-
Missing data	95 (2.9%)	-
Cytogenetics IPSS-R		
Very-good	125 (3.8%)	-
Good	1992 (59.9%)	-
Int	421 (12.7%)	-
Poor	149 (4.5%)	-
Very-poor	254 (7.6%)	-
Missing data	383 (11.5%)	-
IPSS-R risk group		
Very-good	372 (14.6%)	-
Good	1106 (33.3%)	-
Int	630 (19%)	-
Poor	448 (13.5%)	-
Very-poor	372 (11.2%)	-
Missing data	282 (8.5%)	-
Blood counts		
Hemoglobin (g/dL)	-	9.7 (8.6 - 11.2)
Platelets (10^9/L)	-	123 (65 - 229)
ANC (10^9/L)	-	2 (1 - 3.7)
Bone Marrow Blasts %	-	3 (1 - 8)
Missing data	108 (3.2%)	-
Outcome		
Median follow-up (years)[$]	-	3.44
Missing OS data	152 (4.5%)	-
Missing AML data	163 (4.9%)	-

Extended Data Fig. 1 | Study cohort characteristics. Table describing the baseline characteristics of the study cohort. 1Q: first quartile; 3Q: third quartile; OS: overall survival; #: AML classification per WHO 2016 and previously RAEB-T cases. $: Median follow-up time is calculated for censored patients.

Validation cohort (N=1120)		
Characteristic	**No. of cases (%)**	**Median (1Q - 3Q)**
Cohort		
Clinical sequencing	627 (56%)	-
JMPD	314 (28%)	-
JALSG MDS212	179 (16%)	-
Gender		
Male	751 (67%)	-
Female	369 (33%)	-
Age at diagnosis	-	65 (54 - 75)
Missing data	121 (11%)	-
WHO 2016 classification		
MDS		
t-MDS	9 (0.9%)	-
MDS-del5q	7 (0.6%)	-
MDS-SLD	169 (15.1%)	-
MDS-MLD	100 (8.9%)	-
MDS-RS-SLD/MLD	34 (3%)	-
MDS-EB1/2	437 (39%)	-
MDS-U	15 (1.3%)	-
AML		
AML-MRC	121 (10.8%)	-
MDS/MPN		
CMML	43 (3.8%)	-
aCML	4 (0.4%)	-
MDS/MPN-U	6 (0.5%)	-
MDS/MPN-RS-T	4 (0.4%)	-
Missing data	171 (15.3%)	-
IPSS-R risk group		
Very-good	22 (4.2%)	-
Good	60 (11.4%)	-
Int	77 (14.6%)	-
Poor	101 (19.1%)	-
Very-poor	166 (31.4%)	-
Missing data	102 (19.3%)	-
Blood counts		
Hemoglobin (g/dL)	-	8.4 (7.4 - 10.0)
Platelets (10^9/L)	-	76 (39 - 138)
ANC (10^9/L)	-	1.2 (0.5 - 2.4)
Bone Marrow Blasts %	-	6.8 (2 - 15)
Missing data	554 (49%)	-
Outcome		
Median follow-up (years)$	-	1.1
Missing OS data	241 (22%)	-

Extended Data Fig. 2 | Validation cohort characteristics. Table describing the baseline characteristics of the validation cohort. 1Q: first quartile; 3Q: third quartile; OS: overall survival; $: Median follow-up time is calculated for censored patients.

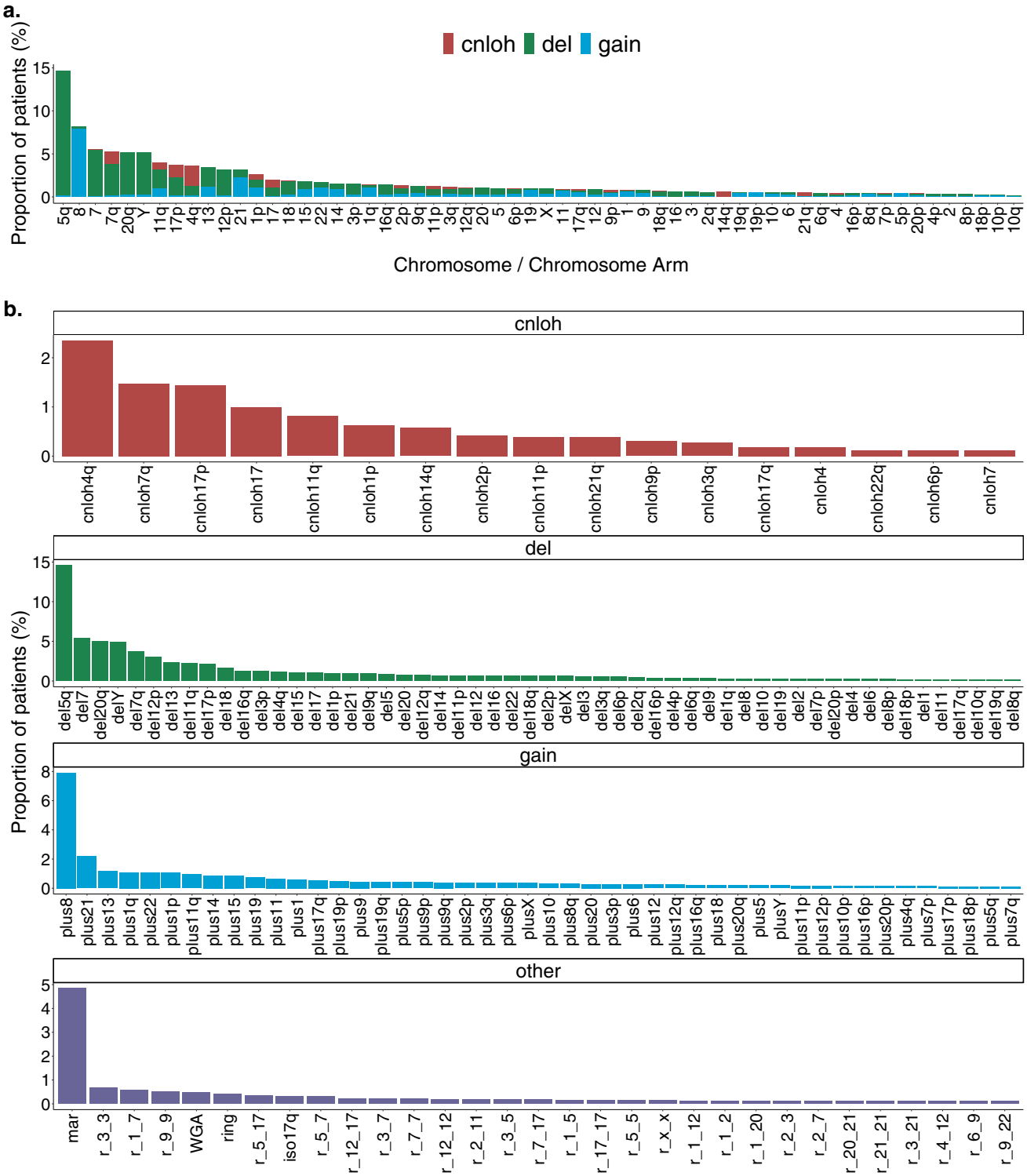

Extended Data Fig. 3 | Landscape of chromosomal aberrations in MDS. a, Landscape of chromosomal arm-level aberrations across 3,324 patients. Aberrations include copy-neutral loss of heterozygosity (cnloh), deletion (del) and gain. Chromosomes or chromosome arms with more than 5 aberrations are depicted on the x-axis. Aberrations were assessed using the integration of conventional G-banding analysis (CBA) data and NGS derived allele specific copy-number profiles (see Methods). NGS aberrant segments were restricted to segments larger than 3 megabases. **b**, Frequency distribution of chromosomal aberrations ordered by type of aberrations. First top three plots represent arm-level copy-neutral loss of heterozygosity (cnloh), deletion (del) and gain. Fourth bottom plot represents other types of aberrations to include the presence of marker chromosome (mar), rearrangements where r_i_j denotes a rearrangement between chromosome i and j, isochromosome 17q (iso17q), whole genome amplification (WGA) and presence of ring chromosome (ring). All aberrations observed in more than 3 patients are depicted. Of note, cnloh is detectable with NGS but not with CBA. On the opposite, rearrangements, presence of marker or ring chromosome and WGA were only assessed from CBA data. In 393 cases with missing CBA data, those specific aberrations were imputed from other molecular markers.

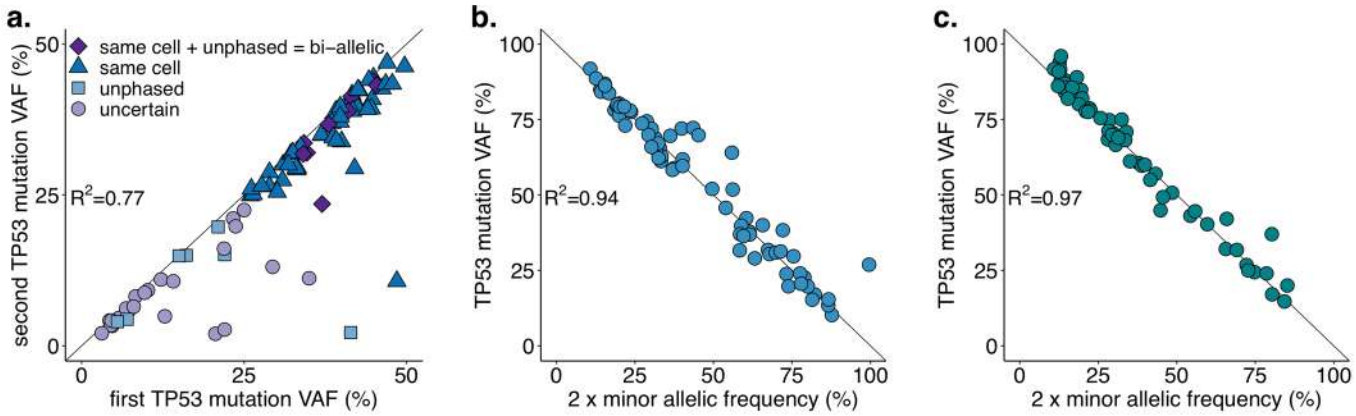

d.

Patient	TP53 Variant 1	Protein Change 1	VAF 1	TP53 Variant 2	Protein Change 2	VAF 2	note
p1	17_7577498_C_T	p.?	0.37	17_7577529_A_T	p.I251N	0.24	
p2	17_7578176_C_T	p.?	0.22	17_7578190_T_C	p.Y220C	0.15	
p3	17_7577538_C_T	p.R248Q	0.16	17_7577570_C_T	p.M237I	0.04	third splice-site mutation at VAF 0.16
p4	17_7577498_C_T	p.?	0.21	17_7577515_T_G	p.T256P	0.2	
p5	17_7577520_A_T	p.I254N	0.46	17_7577539_G_A	p.R248W	0.43	
p6	17_7577106_G_C	p.P278A	0.41	17_7577120_C_T	p.R273H	0.02	
p7	17_7578190_T_C	p.Y220C	0.34	17_7578268_A_C	p.L194R	0.34	
p8	17_7577536_T_A	p.R249W	0.39	17_7577568_C_T	p.C238Y	0.41	
p9	17_7578442_T_C	p.Y163C	0.39	17_7578538_T_A	p.N131I	0.38	
p10	17_7579312_C_T	p.T125T	0.15	17_7579349_A_C	p.F113C	0.15	
p11	17_7578392_C_A	p.E180*	0.05	17_7578403_C_T	p.C176Y	0.06	
p12	17_7578190_T_C	p.Y220C	0.45	17_7578191_A_G	p.Y220H	0.44	
p13	17_7577538_C_T	p.R248Q	0.34	17_7577570_C_T	p.M237I	0.32	
p14	17_7578460_A_C	p.V157G	0.15	17_7578478_G_C	p.P151R	0.65	
p15	17_7578455_C_G	p.A159P	0.04	17_7578524_G_C	p.Q136E	0.07	
p16	17_7577018_C_T	p.?	0.38	17_7577097_C_A	p.D281Y	0.37	
p17	17_7578394_T_A	p.H179L	0.42	17_7578415_AC_A	p.V172fs*2	0.41	
p18	17_7579311_C_T	p.?	0.32	17_7579358_CG_C	p.R110fs*13	0.35	

e.

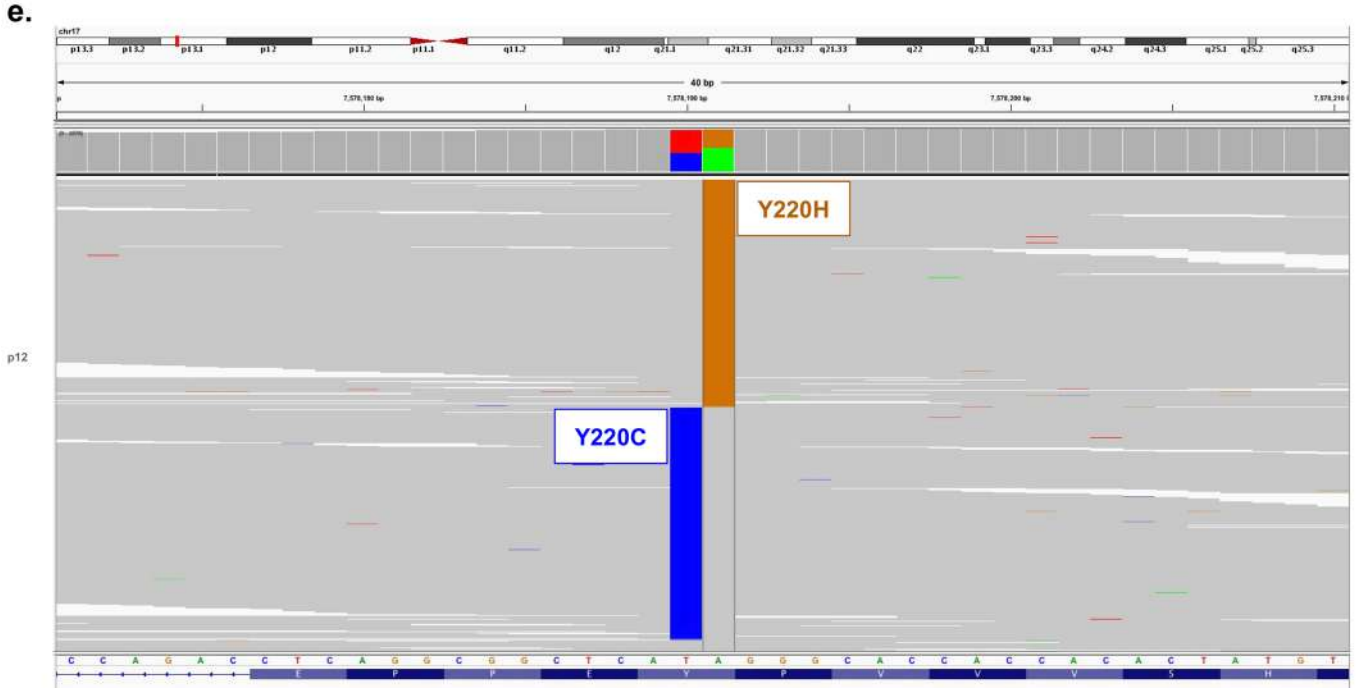

Extended Data Fig. 4 | See next page for caption.

Extended Data Fig. 4 | Evidence of biallelic *TP53* targeting in the cases with multiple *TP53* hits. a, Scatter plot of the two maximum *TP53* variant allele frequency (VAF) values from cases with multiple *TP53* mutations and no copy-neutral LOH or deletion at *TP53* locus (n=90). Points are annotated according to the level of information of the mutation pairs. In 67% (n=60) of pairs the sum of the two VAFs exceeded 50% so that the mutations were considered to be in the same cells as per the *pigeonhole principle* (triangle and diamond points). In 18 cases, the genomic distance between two mutations was within sequencing read length and it was therefore possible to phase the mutations. In all those cases the mutations were observed to be unphased, that is, *in trans* (square and diamond points). Within those 18 pairs of unphased mutations, 10 pairs had a sum of VAFs above 50%, that is, mutations were necessarily on different alleles and in the same cells, implying biallelic targeting (diamond points). **b**, **c**, Scatter plots of the VAF of *TP53* mutations and minor allele frequency of 17p heterozygous SNPs from cases with one *TP53* mutation and 17p deletion (b., n=69) or 17p copy-neutral LOH (c., n=61). The high correlations in (a.), (b.) and (c.) (R^2 of 0.77, 0. 94 and 0.97, respectively) are indicative of biallelic targeting of *TP53*. **d**, Table of pairs of *TP53* mutations from the same patients that could be phased. All pairs were *in trans*, that is, mutations were supported by different alleles. **e**, Representative IGV example of unphased mutations (patient p12 from table (d.)).

Extended Data Fig. 5 | See next page for caption.

Extended Data Fig. 5 | Heatmap of chromosomal aberrations per *TP53* allelic state. Each column represents a patient from the *TP53* subgroups of monoallelic mutation (top orange band, 1mut), multiple mutations (top light blue band, >1mut), mutation(s) and deletion (top blue band, mut+del) and mutation(s) and copy-neutral loss of heterozygosity (top dark blue band, mut+cnloh). Aberrations observed at a frequency higher than 2% in either monoallelic or multi-hit *TP53* state are depicted on the y-axis. Aberrations include from top to bottom the annotation of complex karyotype (complex), the presence of marker chromosome (mar), deletion (del), gain (plus), rearrangement (with r_i_j rearrangement between chromosome i and j), copy-neutral loss of heterozygosity (cnloh), whole genome amplification (WGA) and the presence of ring chromosome (ring). The deletions of 17p of two cases from the 1mut *TP53* subgroup did not affect the *TP53* locus.

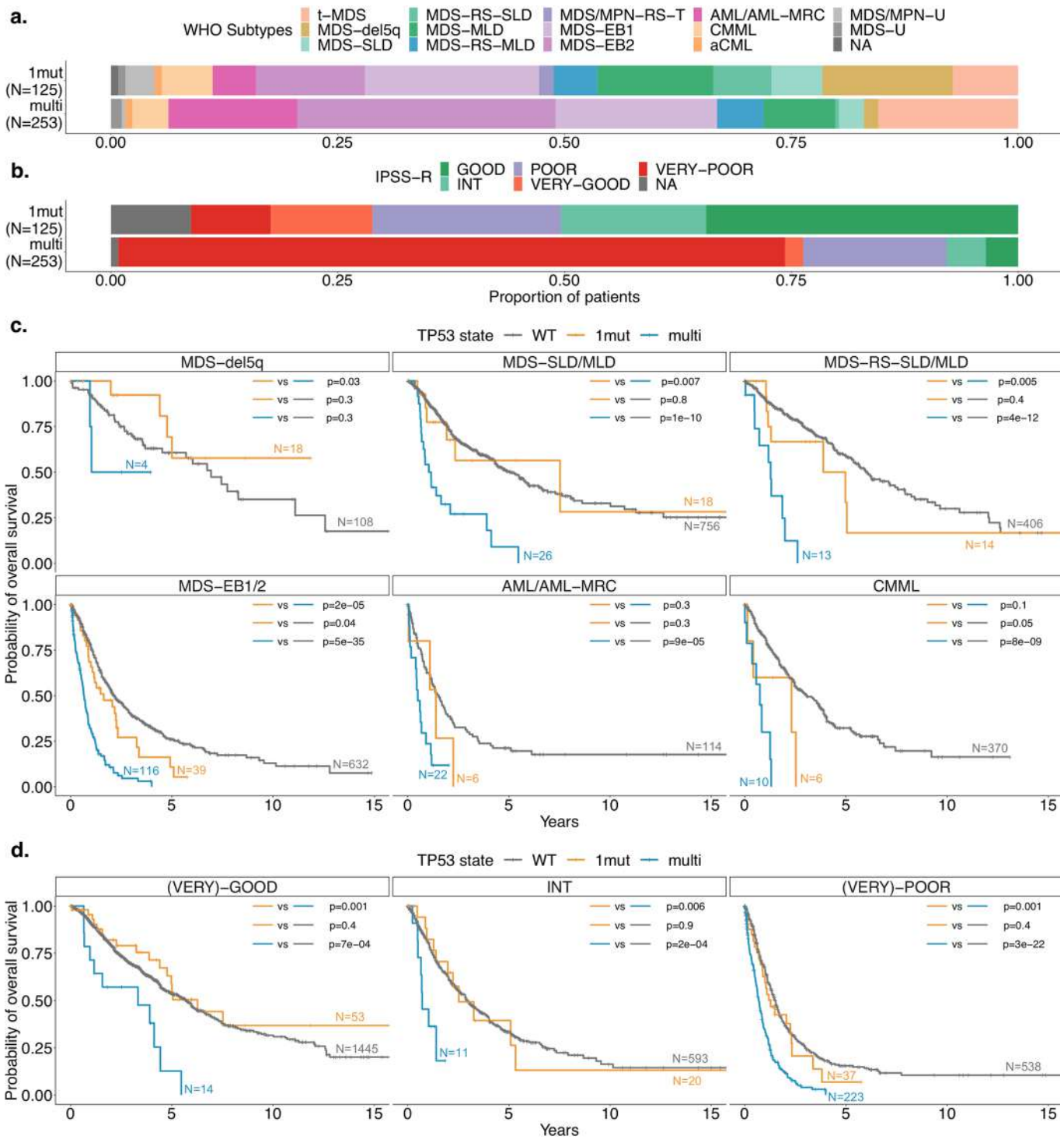

Extended Data Fig. 6 | *TP53* allelic state segregates patient outcomes across WHO subtypes and IPSS-R risk groups. a, Proportion of WHO subtypes per *TP53* allelic state of monoallelic mutation (1mut) and multiple hits (multi). t-MDS: therapy-related MDS; SLD: single lineage dysplasia; RS: ring sideroblast; MLD: multiple lineage dysplasia; EB: excess blasts; AML-MRC: AML with myelodysplasia-related changes; U: unclassified. Multi-hit *TP53* is enriched for t-MDS compared to monoallelic *TP53* state (21% vs. 8%, OR=2.9, p=0.002 two-sided Fisher exact test) and for MDS-EB2 (31% vs. 13%, OR=3.1, $p=5x10^{-5}$ two-sided Fisher exact test). Contrarily, monoallelic *TP53* is enriched for MDS-del5q (15% vs. 2%, OR=8.4, $p=6x10^{-6}$ two-sided Fisher exact test). **b**, Proportion of IPSS-R risk groups per *TP53* allelic state. Multi-hit *TP53* is strongly enriched for the very-poor category compared to monoallelic *TP53* state (74% vs. 9%, OR=28, $p=2x10^{-35}$ two-sided Fisher exact test). **c**, Kaplan-Meier probability estimates of overall survival (OS) across main WHO subtypes per *TP53* allelic state of wild-type *TP53* (WT), monoallelic *TP53* (1mut) and multiple *TP53* hits (multi). WHO subtypes MDS-SLD and MDS-MLD are merged together as MDS-SLD/MLD and WHO subtypes MDS-EB1 and MDS-EB2 are merged together as MDS-EB1/2. **d**, Kaplan-Meier probability estimates of overall survival across IPSS-R risk groups per *TP53* allelic state. IPSS-R very-good and good risk groups are merged together (leftmost panel), and IPSS-R very-poor and poor risk groups are merged together as well (rightmost panel). In (c.) and (d.), annotated p-values are from two-sided log-rank tests and numbers indicate cases with OS data per allelic state.

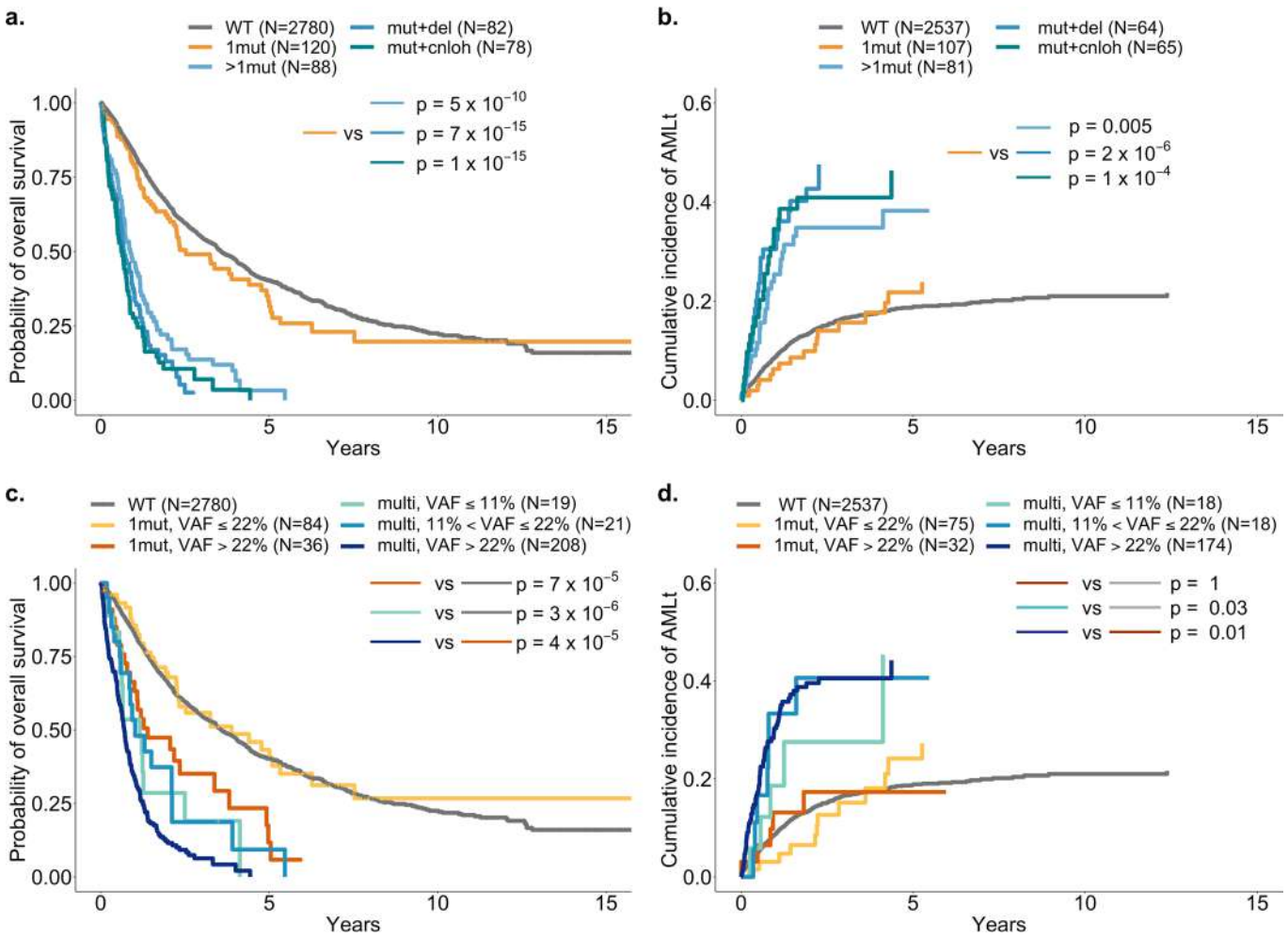

Extended Data Fig. 7 | Outcomes across *TP53* subgroups and VAF strata. a, **b**, Kaplan-Meier probability estimates of overall survival (a.) and cumulative incidence of AML transformation (AMLt) (b.) across *TP53* subgroups of wild-type *TP53* (WT), single *TP53* mutation (1mut), multiple *TP53* mutations (>1mut), *TP53* mutation(s) and deletion (mut+del), *TP53* mutation(s) and copy-neutral loss of heterozygosity (mut+cnloh). **c-d**, Kaplan-Meier probability estimates of overall survival (c.) and cumulative incidence of AMLt (d.) per *TP53* allelic state and range of variant allele frequency (VAF) of *TP53* mutations. Annotated p-values are from two-sided log-rank tests in (a.) and (c.) and from two-sided Gray's tests in (b.) and (d.). The number of cases with outcome data per group is indicated in parentheses.

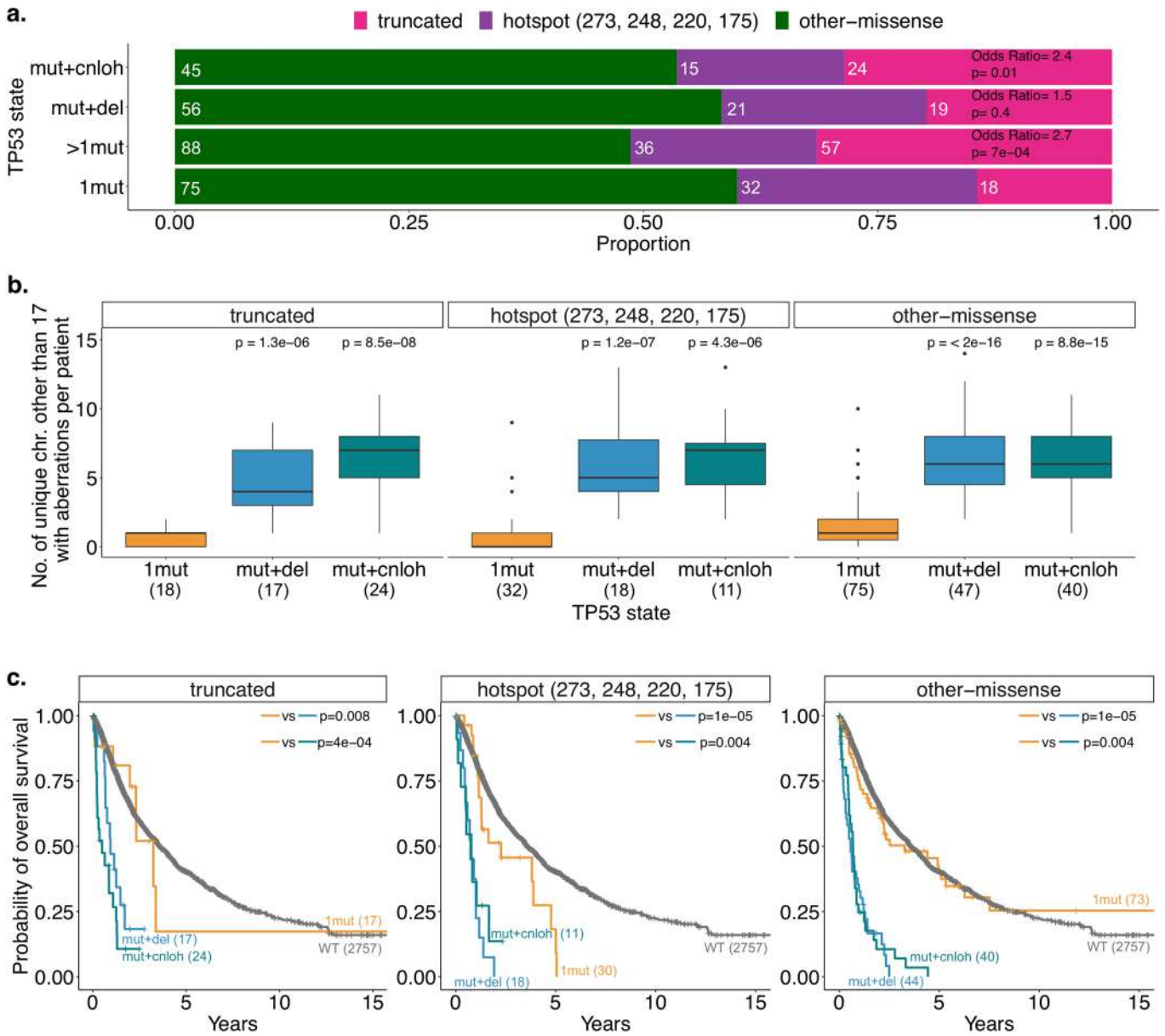

Extended Data Fig. 8 | Maintained differences in genome instability levels and outcomes between *TP53* states per mutation type. a, Proportion of different types of mutation per *TP53* subgroup. Truncated mutations (pink) include frameshift indels, nonsense or nonstop mutations and splice-site variants. Mutations annotated as hotspot (purple) are missense mutations at amino acid positions 273, 248, 220 and 175. Mutations annotated as other-missense (green) are additional missense mutations or inframe indels. Odds ratio and two-sided Fisher's test p-values for the proportion of truncated versus non-truncated mutations between the multi-hit *TP53* subgroups and the monoallelic *TP53* subgroup (1mut) are indicated on the right side. **b**, Number per patient of unique chromosomes other than 17 with aberrations per *TP53* subgroup of single gene mutation (1mut), mutation and deletion (mut+del) and mutation and copy-neutral loss of heterozygosity (mut+cnloh) and across mutation types. Note that 5 patients with both several mutations and deletion or cnloh with ambiguity between the mutation type categories have been excluded for this analysis. The number of patients within each category is indicated in parentheses. In boxplots, the median is indicated by the tick horizontal line, and the first and third quartiles by the box edges. The lower and upper whiskers extend from the hinges to the smallest and largest values, respectively, no further than 1.5x the interquartile range from the hinges. Data beyond the whiskers are plotted individually as dots. The annotated p-values are derived from the two-sided Wilcoxon rank-sum test, each compared to the 1mut group within the same mutation type. **c**. Kaplan-Meier probability estimates of overall survival (OS) per *TP53* subgroup across mutation types. Annotated p-values are from two-sided log-rank tests. The number of cases per subgroup with OS data is indicated in parentheses.

Treated cohort subsets			
	HMA cohort (N=656)	Lenalidomide cohort (N=101)	HSCT cohort (N=310)
Characteristic	**No. of cases (%)**		
TP53 allelic state			
Wild type	511 (78%)	72 (73%)	274 (88%)
Mono-allelic	24 (4%)	12 (12%)	7 (2%)
Multi-hit	121 (18%)	17 (15%)	29 (9%)
TP53 allelic state, with outcome data			
Wild type	497	69	265
Mono-allelic	22	10	7
Multi-hit	119	16	24
Gender			
Male	428 (65%)	35 (35%)	188 (61%)
Female	228 (35%)	66 (65%)	122 (39%)
WHO 2016 classification			
MDS-del5q	4 (0.6%)	50 (50%)	5 (1.6%)
MDS-SLD/MLD	84 (13%)	3 (3%)	59 (19%)
MDS-RS-SLD/MLD	31 (5%)	3 (2%)	21 (6.6%)
MDS-EB1/2	351 (54%)	28 (28%)	144 (46%)
MDS-U	6 (1%)	4 (4%)	7 (2%)
AML/AML-MRC	63 (10%)	6 (7%)	26 (9%)
MDS/MPN	113 (17%)	6 (6%)	45 (14%)
Missing data	4 (0.6%)	1 (0.9%)	3 (0.9%)
Cytogenetics IPSS-R			
Very-good	11 (2%)	-	3 (0.9%)
Good	340 (51%)	63 (63%)	177 (56%)
Int	100 (16%)	6 (6%)	46 (15%)
Poor	58 (9%)	3 (3%)	35 (11%)
Very-poor	111 (17%)	18 (18%)	25 (9%)
Missing data	36 (5%)	11 (11%)	24 (8%)
IPSS-R risk group			
Very-good	19 (3%)	3 (3%)	11 (3%)
Good	95 (14%)	44 (44%)	60 (19%)
Int	151 (23%)	25 (25%)	89 (28%)
Poor	199 (30%)	7 (7%)	87 (28%)
Very-poor	163 (25%)	17 (17%)	50 (17%)
Missing data	29 (4%)	5 (5%)	13 (4%)

Extended Data Fig. 9 | Characteristics of treated cohort subsets. Table describing the baseline characteristics of the subset of patients that i) received hypomethylating agent (HMA), ii) received Lenalidomide in the context of del(5q) or iii) underwent hematopoietic stem cell transplantation (HSCT).

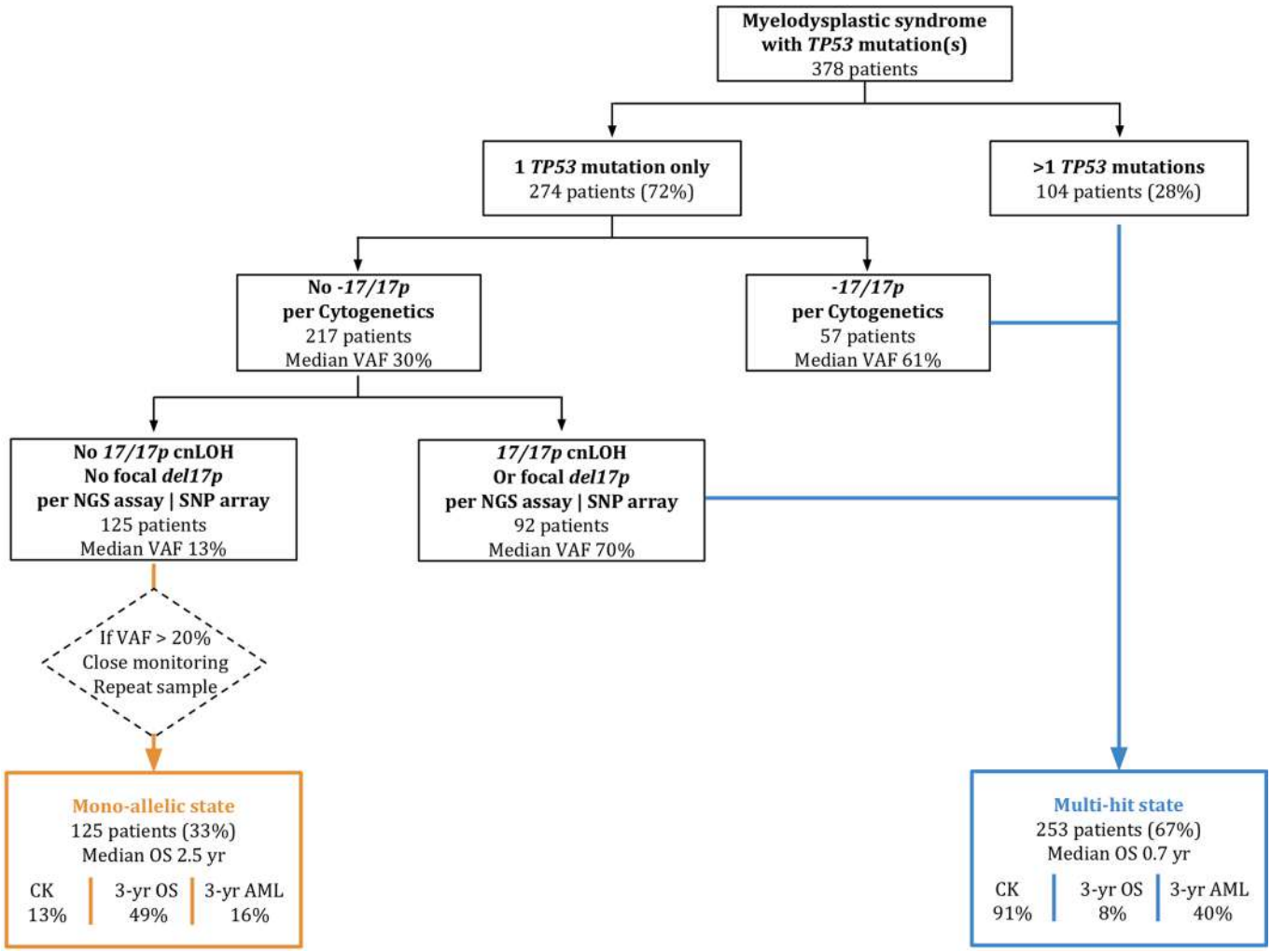

Extended Data Fig. 10 | Clinical workflow for the assessment of *TP53* allelic state. Schematic of a simple clinical workflow based on the number of *TP53* mutations, the presence or absence of deletion 17p per cytogenetic analysis, and the presence or absence of cnLOH or focal deletion at 17p per NGS based assay or SNP array. Mutations were considered if VAF≥2%. VAF: variant allele frequency; CK: complex karyotype; OS: overall survival; AML: transformation to acute myeloid leukemia.

nature research

Corresponding author(s): Elli Papaemmanuil

Last updated by author(s): Jun 15, 2020

Reporting Summary

Nature Research wishes to improve the reproducibility of the work that we publish. This form provides structure for consistency and transparency in reporting. For further information on Nature Research policies, see our Editorial Policies and the Editorial Policy Checklist.

Statistics

For all statistical analyses, confirm that the following items are present in the figure legend, table legend, main text, or Methods section.

n/a	Confirmed
☐	☒ The exact sample size (*n*) for each experimental group/condition, given as a discrete number and unit of measurement
☒	☐ A statement on whether measurements were taken from distinct samples or whether the same sample was measured repeatedly
☐	☒ The statistical test(s) used AND whether they are one- or two-sided *Only common tests should be described solely by name; describe more complex techniques in the Methods section.*
☐	☒ A description of all covariates tested
☐	☒ A description of any assumptions or corrections, such as tests of normality and adjustment for multiple comparisons
☐	☒ A full description of the statistical parameters including central tendency (e.g. means) or other basic estimates (e.g. regression coefficient) AND variation (e.g. standard deviation) or associated estimates of uncertainty (e.g. confidence intervals)
☐	☒ For null hypothesis testing, the test statistic (e.g. *F*, *t*, *r*) with confidence intervals, effect sizes, degrees of freedom and *P* value noted *Give P values as exact values whenever suitable.*
☒	☐ For Bayesian analysis, information on the choice of priors and Markov chain Monte Carlo settings
☒	☐ For hierarchical and complex designs, identification of the appropriate level for tests and full reporting of outcomes
☐	☒ Estimates of effect sizes (e.g. Cohen's *d*, Pearson's *r*), indicating how they were calculated

Our web collection on statistics for biologists contains articles on many of the points above.

Software and code

Policy information about availability of computer code

Data collection	No software was used for data collection.
Data analysis	Alignment: Raw sequence data were aligned to the human genome (NCBI build 37) using BWA version 0.7.17. PCR duplicate reads were marked with Picard tools (https://broadinstitute.github.io/picard/) version 2.18.2. For alignment, we used the pcap-core dockerized pipeline version 4.2.1 available at https://github.com/cancerit/PCAP-core. Sample quality control: Quality control (QC) of the fastq data and bam data were performed with fastQC (http://www.bioinformatics.babraham.ac.uk/projects/fastqc/) version 0.11.5 and Picard tools respectively. Variant calling: Variant were called using a combination of variant callers. For single nucleotide variants, we used Caveman (http:// cancerit.github.io/CaVEMan/) version 1.7.4, Mutect version 4.0.1.2 and Strelka version 2.9.1. For small insertions and deletions, we used Pindel version 1.5.4, Mutect version 4.0.1.2 and Strelka version 2.9.1. Variant allele frequencies were uniformly reported across all called variants using a realignment procedure (https://github.com/cancerit/vafCorrect). Variant annotation: All called variants were annotated with VAGrENT (https://github.com/cancerit/VAGrENT) version 3.3.0 and Ensembl-VEP (https:// github.com/Ensembl/ensembl-vep) with Ensembl version 91 and VEP release 94.5. Copy-number analyses: We assessed chromosomal alterations based on NGS panel sequencing data using CNACS, available at https://github.com/papaemmelab/

toil_cnacs. We also used CNVkit version 0.9.6 (https://cnvkit.readthedocs.io/en/stable/#).

Statistics:
All statistical analyses were conducted using the R statistical platform (R Core Team 2019) (https://www.r-project.org/) version 3.6.1. Kaplan-Meir estimates were computed using the "survival" R package, incidence of AML transformation were estimated using the "cmprsk" R package and Cox proportional hazards regressions were performed using the "coxph" R package.

Reproducibility:
Source code to reproduce analysis is available at https://github.com/papaemmelab/MDS-TP53-state

For manuscripts utilizing custom algorithms or software that are central to the research but not yet described in published literature, software must be made available to editors and reviewers. We strongly encourage code deposition in a community repository (e.g. GitHub). See the Nature Research guidelines for submitting code & software for further information.

Data

Policy information about availability of data

All manuscripts must include a data availability statement. This statement should provide the following information, where applicable:

- Accession codes, unique identifiers, or web links for publicly available datasets
- A list of figures that have associated raw data
- A description of any restrictions on data availability

Clinical, copy-number and mutation data are available at https://github.com/papaemmelab/MDS-TP53-state. The data that underlie Fig1-4 are provided as Source Data.

Databases used in the study are gnomAD https://gnomad.broadinstitute.org, COSMIC https://cancer.sanger.ac.uk/cosmic, cBioPortal for Cancer Genomics https://www.cbioportal.org, OncoKB Precision Oncology Knowledge Base https://www.oncokb.org, ClinVar https://www.ncbi.nlm.nih.gov/clinvar and IARC TP53 Database https://p53.iarc.fr.

Field-specific reporting

Please select the one below that is the best fit for your research. If you are not sure, read the appropriate sections before making your selection.

☒ Life sciences ☐ Behavioural & social sciences ☐ Ecological, evolutionary & environmental sciences

For a reference copy of the document with all sections, see nature.com/documents/nr-reporting-summary-flat.pdf

Life sciences study design

All studies must disclose on these points even when the disclosure is negative.

Sample size	No statistical methods were used to predetermine sample size; all 3,324 available samples that passed quality control were utilized.
Data exclusions	We initially considered 4,105 MDS patient samples, and after quality control (QC) of the samples we excluded 781 samples and report results on 3,324 samples. QC included: - Evaluation of duplicate samples from SNP fingerprinting - Concordance between coverage sequencing data and clinical data (sex, cytogenetics) - Exclusion of treated samples (N=131) as the study focuses on MDS at diagnosis - Exclusion of pediatric cases (N=3) as the study focuses on adult de-novo MDS.
Replication	We validated results on an independent cohort of 1,120 MDS patients samples collected by the Japanese MDS consortium.
Randomization	This is not relevant to the study, no experimental group allocation.
Blinding	Blinding was not relevant to the study, as there was no control and treatment arms involved.

Reporting for specific materials, systems and methods

We require information from authors about some types of materials, experimental systems and methods used in many studies. Here, indicate whether each material, system or method listed is relevant to your study. If you are not sure if a list item applies to your research, read the appropriate section before selecting a response.

Materials & experimental systems

n/a	Involved in the study
☒	☐ Antibodies
☒	☐ Eukaryotic cell lines
☒	☐ Palaeontology and archaeology
☒	☐ Animals and other organisms
☐	☒ Human research participants
☐	☒ Clinical data
☒	☐ Dual use research of concern

Methods

n/a	Involved in the study
☒	☐ ChIP-seq
☒	☐ Flow cytometry
☒	☐ MRI-based neuroimaging

Human research participants

Policy information about studies involving human research participants

Population characteristics	Covariate population characteristics: - Age at diagnosis - Time from diagnosis to sample collection - Gender - Bone marrow blasts count - Hemoglobin level - Platelet level - Neutrophil count - Cytogenetic and Cytogenetic risk group - IPSS-R risk score - Diagnostic WHO 2016 subtype - Time from diagnosis to treatment - Type of disease modifying treatment received - Time from diagnosis to AML transformation - Overall survival - Vital status
Recruitment	All patients with a diagnosis of myelodysplastic syndromes or closely related myeloid neoplasms at any of the partner institutions were eligible for and consented for the study. No exclusionary criteria existed. Patient's samples had to be either diagnostic or ascertained prior to the patient receiving disease modifying treatments that could alter the molecular and clonal inferences.
Ethics oversight	Samples were obtained with informed consent in accordance with the Declaration of Helsinki and appropriate ethics committee approval from each partner institution. Partner institutions that obtained ethical approval from ethical committees are: Memorial Sloan Kettering Cancer Center. Karolinska Institute. Dusseldorf MDS Registry. University of Pavia. Le Fe University Hospital. Radboudumc Medical Center Nijmegen. Cochin Hospital. Chang Gung Memorial Hospital. Gruppo Romano Laziale MDS. University of Bologna. Medical University of Vienna. Hannover Medical School. University Hospital Dresden. Federal University of Ceara. Institut Josep Carreras. Aou Careggi Hospital. Democritus University of Thrace. University of Oxford. Hospital Isrealita Albert Enstein. Vanderbilt University. Institute of Hematology and Blood Transfusion. University Medicine Gottingen. Rete Hemtologica Lombarda. Saint Louis Hospital.

Note that full information on the approval of the study protocol must also be provided in the manuscript.

Clinical data

Policy information about clinical studies

All manuscripts should comply with the ICMJE guidelines for publication of clinical research and a completed CONSORT checklist must be included with all submissions.

Clinical trial registration	Not a clinical trial
Study protocol	*Note where the full trial protocol can be accessed OR if not available, explain why.*
Data collection	*Describe the settings and locales of data collection, noting the time periods of recruitment and data collection.*
Outcomes	*Describe how you pre-defined primary and secondary outcome measures and how you assessed these measures.*